Chemistry–A European Journal
Review
doi.org/10.1002/chem.202402629
Chemistry Europe
European Chemical Societies Publishing
www.chemeurj.org

Simultaneous Photocatalytic CO_2 Reduction and H_2O Oxidation Under Non-Sacrificial Ambient Conditions

Qing Tong[+],[a] Yu Tang[+],[a] Weixin Zou,*[a] Yu-Xin Ye,[b] Lin Dong,[a] and Gangfeng Ouyang*[c]

The utilization of CO_2, H_2O, and solar energy is regarded as a sustainable route for converting CO_2 into chemical feedstocks, paving the way for carbon neutrality and reclamation. However, the simultaneous photocatalytic CO_2 reduction and H_2O oxidation under non-sacrificial ambient conditions is still a significant challenge. Researchers have carried out extensive exploration and achieved dramatic developments in this area. In this review, we first primarily elucidate the principles of two half-reactions in the photocatalytic conversion of CO_2 with H_2O, i.e., CO_2 reduction by the photo-generated electrons and protons, and H_2O oxidation by the photo-generated holes without sacrificial agents. Subsequently, the strategies to promote two half-reactions are summarized, including the vacancy/facet/morphology design, adjacent redox site construction, and Z-scheme heterojunction development. Finally, we present the advanced in situ characterizations and future perspectives in this field. This review aims to provide fresh insights into effectively simultaneous photocatalytic CO_2 reduction and H_2O oxidation under non-sacrificial ambient conditions.

1. Introduction

With the rapid growth of social economy and population, there is an enormous increase in the need for production.[1–3] The utilization of fossil fuels, along with ubiquitous anthropogenic activities, generates a massive flood of carbon dioxide (CO_2) emissions.[4] In past year, there has been a significant increase of 1.1% in the global energy-related CO_2 emissions, reaching an unprecedented level of 37.4 billion tons. Aimed at mitigating the environmental impact of excessive CO_2 emissions contributing to global climate change and related environmental challenges, the carbon capture, utilization, and storage (CCUS) has emerged as a key technology.[5] One promising method is photocatalytic CO_2 reduction (CO_2RR), using renewable solar energy to convert concentrated CO_2 into high-value chemical feedstocks, which simultaneously achieves carbon neutrality and resource valorization, thereby improving the global carbon cycle. Recently, the field of photocatalytic CO_2 reduction has achieved a significant progress, and is summarized in the previous reviews.[6–9,10–13]

Although a great progress has been made in the photocatalytic conversion of CO_2, the simultaneous photocatalytic CO_2 reduction and H_2O oxidation remains a great challenge, due to the complex reaction process and high activation energy of CO_2 molecules. In addition, enhancing the process of the H_2O oxidation by holes can promote the CO_2 reduction to carbonaceous products by electrons.[14–19] Therefore, the proton donation from H_2O dissociation and the sluggish kinetics of H_2O oxidation ($E = 1.23$ V vs. RHE) are also the determining factors for the overall photocatalytic CO_2 reduction reaction.[20–21] Generally, the costly sacrificial agents coupled with photosensitizers could consume holes, and are used to improve the photocatalytic efficiency of CO_2 conversion, which inevitably escalates the experimental cost and limits its wider practical application.[22–28] Based on that, the simultaneous photocatalytic CO_2 reduction and H_2O oxidation under non-sacrificial ambient conditions is of great importance and highly desirable, which is an environmentally friendly approach to solar energy utilization and CO_2 conversion, and is the ultimate goal of photocatalytic CO_2 utilization.

Herein, an overview of the developments and challenges in the simultaneous photocatalytic CO_2 reduction and H_2O oxidation under non-sacrificial ambient conditions in recent is present. To begin, two half-reaction mechanisms of photocatalytic CO_2 reduction and H_2O oxidation are described, respectively. Within this context, the multi-step proton-coupled electron transfer processes competing hydrogen evolution reactions,[29] various product stoichiometries and electrochemical potentials,[30–31] and different catalytic pathways in the photocatalytic half-reaction of CO_2 reduction are highlighted. For another photocatalytic half-reaction of H_2O oxidation, the factors contributing to the sluggish kinetics are elucidated. Subsequently, we outline recent strategies for efficient simultaneous CO_2 reduction and H_2O oxidation. This section summarizes the comprehensive strategies aimed at increasing the efficiency of photocatalytic CO_2 conversion, including vacancy/

[a] Q. Tong,[+] Y. Tang,[+] W. Zou, L. Dong
State Key Laboratory of Pollution Control and Resource Reuse, School of the Environment, Key Laboratory of Mesoscopic Chemistry of MOE, School of Chemistry and Chemical Engineering, Jiangsu Key Laboratory of Vehicle Emissions Control, Center of Modern Analysis, Nanjing University, Nanjing 210023, P. R. China
E-mail: wxzou2016@nju.edu.cn
[b] Y.-X. Ye
School of Chemical Engineering and Technology, IGCME, Sun Yat-sen University, Zhuhai 519082, P. R. China
[c] G. Ouyang
Key Laboratory of Bioinorganic and Synthetic Chemistry of Ministry of Education, LIFM, School of Chemistry, IGCME, Sun Yat-sen University, Guangzhou 510006, P. R. China
E-mail: cesoygf@mail.sysu.edu.cn
[+] Qing Tong and Yu Tang contributed equally to this work.

facet/morphology design, adjacent redox site construction, and Z-scheme heterojunction development. In addition, we provide a summary of advanced characterizations for revealing reaction mechanisms. An overview of techniques used to explore the photocatalytic mechanisms for CO_2 reduction and H_2O oxidation, including in situ spectroscopy, theoretical calculations, etc., are summarized in this section. Finally, we highlight a forward-looking perspective on the outstanding challenges and opportunities, such as, accurate characterizations for active sites, efficient practical application in photocatalysis, etc. This review would provide guiding recommendations in the field of the photocatalytic CO_2 conversion under non-sacrificial ambient conditions.

2. Fundamentals and Challenges of Photocatalytic CO_2 Reduction and H_2O Oxidation

1.2. Principles for semiconductor-based photocatalysis

A semiconductor material is defined by its mesoscopic electronic conductivity, which lies between conductors and insulators. Within this crystalline lattice framework, the valence and conduction bands as salient energy spectrums affect coordinating interactions of electronic configurations and charge transport. Specifically, the valence band represents the top of occupied quantum states, while the conduction band is the bottom of unoccupied quantum states, which profoundly affects the electrical properties of the material. As shown in Figure 1a, the light with a photon energy equal to or higher than the band gap of the semiconductor is absorbed, inducing the electron transferring from the valence band maximum (VBM) to the conduction band minimum (CBM), and simultaneously generating holes at the VBM.[32] The photon-generated electrons and holes then migrate distinctly to the catalyst surface, which interact with the absorbed reactants, for example, CO_2 is reduced by photon-generated electrons to hydrocarbons, and H_2O is oxidized by holes into O_2 or H_2O_2 on the oxidation sites.[33–34]

Thermodynamically, the theoretical potential position for the reduction half-reaction should be below the conduction band edge, whereas for the oxidation half-reaction, it should be above the valence band edge (Figure 1a). In the reported catalysts, the heterojunction becomes effective with the broad-spectrum responsiveness and promoted charge separation.[35] Based on the direction of charge transfer, the heterostructures can be categorized into Type II junctions and Z-scheme structures (Figure 1b and 1c).[36–39] In the Type II junctions, the migration processes of high-energy photoexcited electrons and holes towards neighboring semiconductors occur spontane-

Qing Tong is a Senior Engineer at Center of Modern Analysis of Nanjing University. She received her Ph.D. in Chemistry from Nanjing University in 2016 under the supervision of Prof. Yining Fan. Her current research interests include the design and characterization of nanomaterials for catalytic elimination of volatile organic pollutants, and resource utilization of carbon dioxide.

Yu Tang is currently a Ph.D. student at School of Chemistry and Chemical Engineering of Nanjing University. He received his B.S. in Chemistry from Nanjing University in 2022. His research is focused on the photoelectrocatalysts, and the photoelectrocatalytic NO_3RR and C-N coupling reaction.

Weixin Zou is an Associate Professor at School of the Environment of Nanjing University. She received her Ph.D. in Chemistry from Nanjing University in 2015 under the supervision of Prof. Lin Dong. She was a Postdoc from 2016 to 2019 in Nanjing University. Her current research interests include the development of environmental catalytic materials, and their applications in catalytic gas pollutant removal, and carbon dioxide conversion.

Gangfeng Ouyang is a Professor of Chemistry at Sun Yat-sen University. He received his Ph.D. in Physical Chemistry from Sun Yat-sen University in 2003 under the supervision of Prof. Beisheng Kang. He was a Postdoc at the University of Waterloo, Canada in the group of Prof. Janusz Pawliszyn. He was a winner of the National Science Found for Distinguished Young Scholars and Distinguished Professor of "Zhujiang Scholar". Currently, his research is focused on the design of new functional materials for biocatalysis, photocatalysis and environmental analysis.

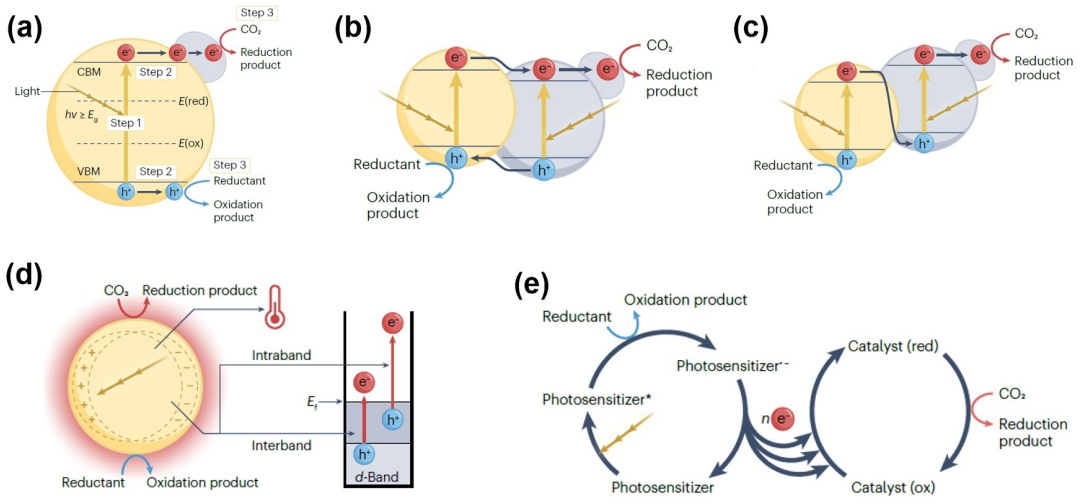

Figure 1. (a) The photo-induced reduction and oxidation reactions based on a semiconductor. Typical structures for simultaneous photocatalytic CO_2 reduction and H_2O oxidation: (b) a Type II heterostructure, (c) a Z-scheme heterostructure, (d) a metallic photocatalyst with the localized surface plasmon resonance, and (e) a molecular catalyst coupled with a photosensitizer.[33] Copyright 2023, Springer Nature.

ously, moving towards conduction and valence bands with lower energy levels,[40–42] respectively, as illustrated in Figure 1b. As a result, the electrons involved in the reduction reaction and the holes participating in the oxidation reaction are largely separated onto two different semiconductors, i.e., reduction and oxidation sites, effectively solving the problem of electron-hole recombination that usually occurs on single-component semiconductors after photoexcitation. Therefore, the Type II junction is an ideal choice compared to a single-component semiconductor. Different form Type II junctions, Z-scheme heterojunctions are provided with a wider light absorption range. Moreover, their electrons on lower conduction band are injected into holes on valence band of another component with a higher position (Figure 1c),[43–45] resulting in a stronger oxidation-reduction ability. As for determining the type of heterojunction, a comprehensive consideration including semiconductor types, valence and conduction band positions, as well as the direction of band bending is necessary,[46] which have been summarized in the previous review.[11]

Besides the heterojunction photocatalysts, the specific metallic nanoparticles, including Cu, Au, Ag, Bi, etc., with the localized surface plasmonic resonance (LSPR) phenomena, i.e., the collective oscillation of external electrons after the injection of photons with resonant frequency, could have enhanced electromagnetic field, improving the efficiency and lifetime of photo-generated charges (Figure 1d).[47–49] When occurring on plasmonic metals, the localized heating leads to the generation of carriers with higher energy levels, referred to "hot charge carriers", together with a larger Fermi level and a stronger surface electronic field. Therefore, these factors exert a superior catalytic facilitation towards the photocatalytic CO_2 reduction and H_2O oxidation, especially from an energetic point of view. Moreover, the homogeneous photocatalytic steps involving so-called photosensitizers and molecular catalysts are also briefly introduced.[50–51] As shown in Figure 1e, upon excitation of the photosensitizer, the immediate quenching occurs as H_2O molecules immediately occupy empty orbitals, resulting in H_2O oxidation to the product of O_2 or H_2O_2. Simultaneously, the excited and negatively charged photosensitizer transfers electrons to the LUMO of the molecular catalyst, and then participates in the CO_2 reduction reaction. As a result, the oxidation-reduction cycle was formed.

2.2. Photocatalytic half-reaction of CO_2 reduction

In the photocatalytic CO_2 reduction, the reactant molecule of CO_2 is a linear and non-polar configuration, with a C–O bond length of 116 pm, which locates between that of C=O bonds (124 pm) and C≡O bonds (113 pm). And its bond energy of 803 kJ/mol exhibits a certain degree of triple-bond characteristic.[52–53] As displayed in Figure 2a, the s orbital of C hybridizes with one p orbital to form two s-p hybrid orbitals in a linear distribution. These s-p hybrid orbitals each overlap "end-to-end" with the p orbitals of O to form two σ bonds, and the remaining two unhybridized p orbitals of C lie on either side of the s-p hybrid orbitals and overlap "side-by-side" with the p orbitals of O to form delocalized π bonds. Due to the above-mentioned electronic structures of the CO_2 molecule, the C atom acts as an electron-deficient center, possessing lower-energy empty orbitals of $2\pi_u$, thereby giving it a higher electron affinity and making it relatively more prone to accept electrons to be reduced to hydrocarbons.

There are various products of CO_2RR, such as CO,[56–58] CH_3OH,[59–60] CH_4,[61–62] HCOOH,[63] C2H5OH,[64] etc. with different theoretical redox potentials.[65–66] In general, the differences in reaction pathways and the number of transferred electrons would lead to various reduction products, which in most cases are primarily determined by the intrinsic properties of the photocatalysts.[67] For example, the binding energy of carbonaceous intermediates on the material surface determines whether it proceeds to further hydrogenation steps or

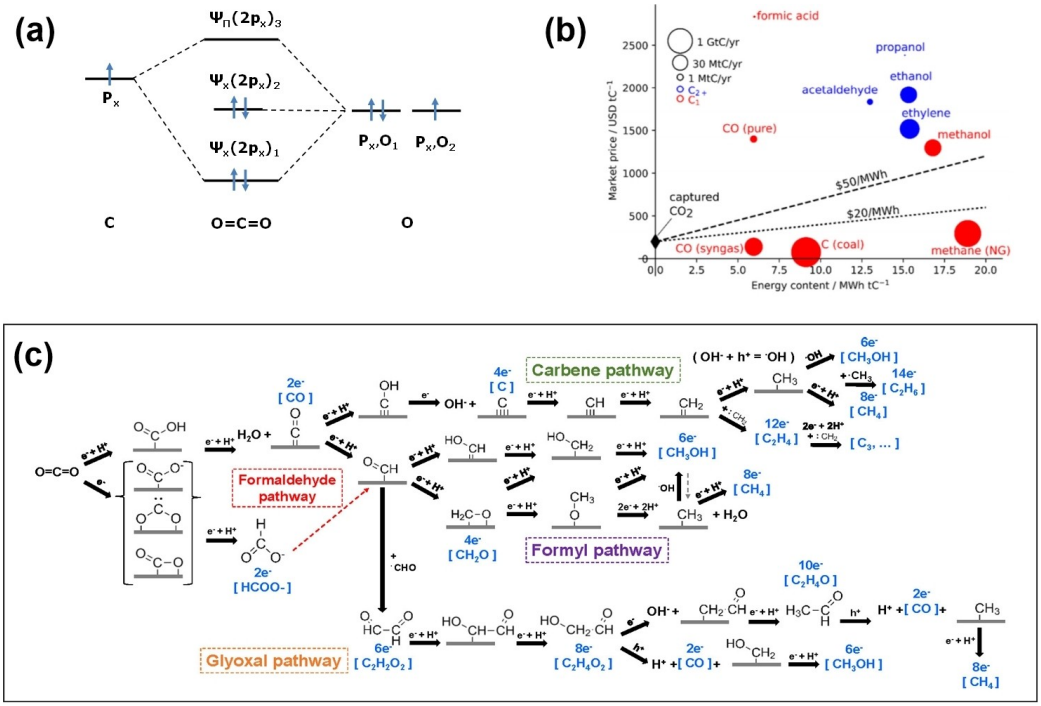

Figure 2. (a) CO_2 molecular orbital.[54] Copyright 2017, Wiley-VCH. (b) Energy density, market price and annual yield of various CO_2RR products (dotted lines represent minimum cost prices for energy consumption based on different commercial technologies).[55] Copyright 2019, American chemical society. (c) The proposed pathways of photocatalytic CO_2RR for C_1 and C_2 products.[10] Copyright 2022, American chemical society.

desorption directly to form products. It has been reported that for the electrochemical CO_2RR, some elements are showed to be able to yield certain specific products, e.g. Bi,[68–69] Sn,[70] In,[71] Pb[72] for the HCOOH product; Au,[73] Ag,[74] Pd[75] for CO, and Cu[76–77] for C_{2+} products with over 90% Faraday efficiency, due to suitable adsorption energies. Unfortunately, in the field of photocatalytic CO_2 conversion, there is a lack of guidance on the relationship between the photocatalyst and selectivity.[78–79] The same material exhibits a contrast in product selectivity between photocatalysis and electrocatalysis for CO_2 reduction. Besides the thermodynamic factors, variations in energy input methods and reaction environments play an important role, resulting in uncontrollable kinetic factors that make the products corresponding to a given material unpredictable. Based on our experience, alloy materials containing noble metals tend to facilitate the generation of CH_4,[80] possibly due to the enhanced dissociation ability of H_2O, thereby promoting active hydrogen or proton transfer; some 2D materials are more able to produce CH_3OH or C_2H_5OH, resulted from the ultrafast carrier separation and transfer.[60,81] Among the various products of photocatalytic CO_2 reduction (Figure 2b), the higher value hydrocarbons such as formic acid (C1) and ethylene (C2) are considered prominent, as well as the heavy demand for synthesis gas and methane, which is advantageous for photocatalytic CO_2 reduction, as most reported catalysts favor to CO or CH_4. However, to date, the yield rate of the photocatalytic CO_2 reduction is limited by the poor quantum efficiency of semiconductors, which should be solved if further the progress towards industrial scale is realized.

In addition, the photocatalytic CO_2 reduction is a complex reaction process involving the transfer of multiple electrons and protons transfer. Theoretical studies suggest of three fundamental processes: molecular adsorption and activation, proton and electron transfer coupled with hydrogenation and deoxygenation, and finally desorption of product molecules.[82–84] In a previous review, Habisreutinger et al.[85] used TiO_2 as a model catalyst to investigate the principles underlying the formation of certain C1 and C2 products, termed the carbene, glyoxal and formaldehyde pathways, respectively, as illustrated in Figure 2c. Contrary to the conventional wisdom, in addition to the proton-coupled electron transfer (PCET) processes, some can be driven by the transfer of single electron and proton (sometimes holes or hydroxyl), which makes the final products unpredictable. This indeterminacy depends on the binding modes of CO_2 on the catalyst surface, e.g., carbon coordination, oxygen coordination or mixed coordination. Different adsorption energies for a common intermediate, such as *COOH, *CO, *CHO, etc. can induce distinct reaction pathways. Moreover, some side reactions such as hydrogen evolution reaction (HER) would occur, if superfluous H_2O reduction and optimal *H binding energy are achieved. Therefore, a deep understanding of the underlying principles is required to elucidate the reaction pathways for CO_2 reduction, and we aim to further elucidate the relationships between the photocatalyst and reaction selectivity in the future, which is of paramount significance for the photocatalytic CO_2 reduction.

2.3. Photocatalytic half-reaction of H_2O Oxidation

For the photocatalytic CO_2 reduction reaction without sacrificial reagents, the reduction half-reaction involves photoelectrons and CO_2, and the holes are consumed by the H_2O reactant for a complete overall reaction. However, much effort has been put into CO_2 reduction to achieve satisfactory performance, overlooking the involvement and importance of H_2O oxidation.[86–88] In fact, the well-regulated relationship between two half-reactions is the guarantee for charge equilibrium.[89] If the rate of the reduction half-reaction is significantly lower than that of the oxidation half-reaction, it will lead to the accumulation of electrons and holes, thereby affecting the reaction rates.

The design of the photocatalysts with an excellent performance should consider both aspects of CO_2 reduction and H_2O oxidation simultaneously. Generally, H_2O oxidation has slower kinetics than CO_2RR, because its theoretical potential of 1.23 V vs. RHE is much higher. Therefore, many reports have used sacrificial agents, such as Na_2SO_3, to replace H_2O oxidation and could further improve the performance by an order of magnitude. However, the introduce of sacrificial agents in the photocatalytic CO_2 reduction is expensive and environmentally unfriendly. Therefore, it is imperative to explore and summarize the mechanism of H_2O oxidation in the photocatalytic CO_2 reduction, which to our knowledge is the first systematic overview of the simultaneous photocatalytic CO_2 reduction and H_2O oxidation under non-sacrificial ambient conditions.

A distinct route for H_2O oxidation undergoes $*H_2O \rightarrow *OH \rightarrow *O \rightarrow *OOH \rightarrow O_2$, as a typical model for both electrochemical oxygen evolution reaction (OER)[90] and photocatalytic H_2O oxidation,[91] as illustrated in Figure 3a. It is noteworthy that the proton formation during the dehydrogenation process of H_2O molecules serves as a crucial proton source for CO_2 reduction,[92] which again emphasizes the importance of promoting H_2O oxidation. For metal oxide catalysts, there are two types of mechanisms for H_2O oxidation, referred to adsorbate evolution mechanism (AEM) and lattice oxygen oxidation mechanism (LOM), respectively.[93] Unlike the AEM pathway, the LOM involves the O_2 formation from lattice oxygen (O_{lat}) and *O on the oxide surface, followed by desorption, while oxygen from H_2O is converted to O_{lat} on the oxide surface as a replenishment, similar to the MvK mechanism, and the phenomenon and mechanism are applicable to the H_2O oxidation in photocatalysis and electrocatalysis. For the electrocatalysis, it involves the direct gain and loss of electrons at the two electrodes by the applied voltage, whereas the photocatalysis uses holes to extract electrons from H_2O, considered as the process of H_2O oxidation, which is related to the surface properties of the catalyst. For example, the oxygen vacancies could facilitate hydrolysis and simultaneously activate the adsorbed CO_2 and H_2O molecules,[94] as shown in Figure 3b. Furthermore, based on current commercial alkaline electrolyzers, the noble-metal-based catalysts usually exhibit excellent capability for H_2O oxidation. The Au-OOH and Ru-OOH exhibit lower formation energies, leading to the successful achievement of the H_2O oxidation (Figure 3c and 3d).[91,95] Based on the extensive research on the electrocatalytic OER, the modulation of its kinetics can accelerate the reaction rate of hydrogen evolution reaction (HER). Similarly, this concept can be applied to photocatalytic CO_2 reduction, through the promotion of H_2O oxidation to accelerate CO_2 reduction,[92] as shown in Figure 3e.

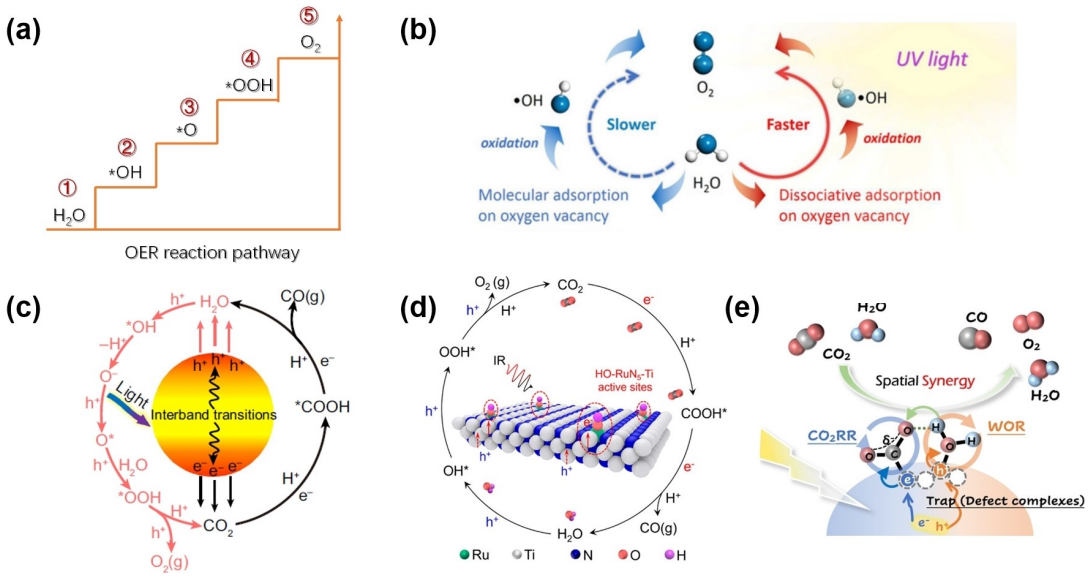

Figure 3. (a) The reaction intermediates for OER.[93] Copyright 2020, American chemical society. (b) Oxygen vacancies for the enhanced photocatalytic H_2O oxidation.[94] Copyright 2016, American chemical society. The reaction pathways for photocatalytic CO_2 reduction and H_2O oxidation on (c) Au nanoparticles,[91] Copyright 2022, Springer Nature. And (d) HO–Ru/TiN.[95] Copyright 2023, American chemical society. (e) Scheme diagram of spatial synergistic half-reactions in photocatalytic CO_2 reduction by H_2O.[92] Copyright 2024, Wiley-VCH.

3. Strategies for Efficiently Simultaneous CO_2 REDUction and H_2O Oxidation

In recent years, the importance of H_2O oxidation in the photocatalytic CO_2 reduction has been gradually recognized, and a significant progress is made in improving photocatalytic performance under non-sacrificial ambient conditions. In general, the advanced material construction plays a key role in the efficient CO_2 reduction and H_2O oxidation, and thus various strategies have been carried out, such as vacancy/facet/morphology design, adjacent redox site construction, and Z-scheme heterojunction development. In this section, we provide a detailed description of the characteristics and applications of each strategy through the typical examples, and the corresponding catalytic performances (reaction conditions, products, apparent quantum yields AQY) are summarized comprehensively in Table 1, in order to provide a better understanding of the efficient strategies for photocatalytic CO_2 reduction under non-sacrificial ambient conditions.

3.1 Vacancy/Facet/Morphology Design

3.1.1. Vacancy

The presence of vacancies in the photocatalyst is able to effectively improve the photocatalytic performance, because the introduction of anionic vacancies into the crystal structure can simultaneously generate unsaturated defects, which serve as appropriate and active sites for CO_2 adsorption and H_2O activation. For example, Li et al.[94] proposed that in order to promote CO_2 photoreduction, the activation and oxidation of H_2O was important, which was closely related to the hole trapping ability of the catalyst associated with oxygen vacancy (O_v). The surface O_v species is used to promote the separation of photogenerated electrons and holes, which usually exists the edged amorphous layer and atomic defects.[98] The synthesized In/TiO_2 catalyst enriched with O_v was showed the In as the active site for CO_2 adsorption and activation, and the O_v site for H_2O oxidation.[99]

Various methods have been designed and applied to generate vacancies in the photocatalysts, such as thermal/plasma treatment to remove lattice oxygen atoms, doping impurities for crystal asymmetry, etc. For example, Yin et al.[96] reported that a series of SnS_2 with different S-vacancy (V_s) ratios could be synthesized by prolonged Ar-plasma treatment time, and the appropriate V_s (23.07 %) ensured the integrity of the crystal structure while maintaining the optimal activation capability. In addition, the in situ generated O_v in S-doped BiOCl was used to facilitate H_2O and CO_2 adsorption, in which S sites enhanced H_2O dissociation and proton transfer, and the $S_{0.3}$-BiOCl showed a multiple-fold increase in performance compared to others.[97] However, to date, many literatures on the photocatalytic CO_2 reduction with H_2O have focused on the anionic vacancies, while the limited research has been carried out on the cationic vacancies. We believe that the influence of cationic vacancies on the photocatalytic CO_2 reduction and H_2O oxidation would be unexpected and amazing.

3.1.2. Facet

The facet engineering with different surface atomic arrangements and coordination environments has been considered as an ideal strategy, which facilitates the light absorption, separation of photogenerated charges, and reactant adsorption.[126–129] Cheng et al.[130] reported a study on the facet effect of MOFs, where the NH_2-MIL-125(Ti) was synthesized with different ratios of (001) and (111) facets (Figure 4a), and it was found that the only (111) facets present in the octahedron exhibited better performance than others.

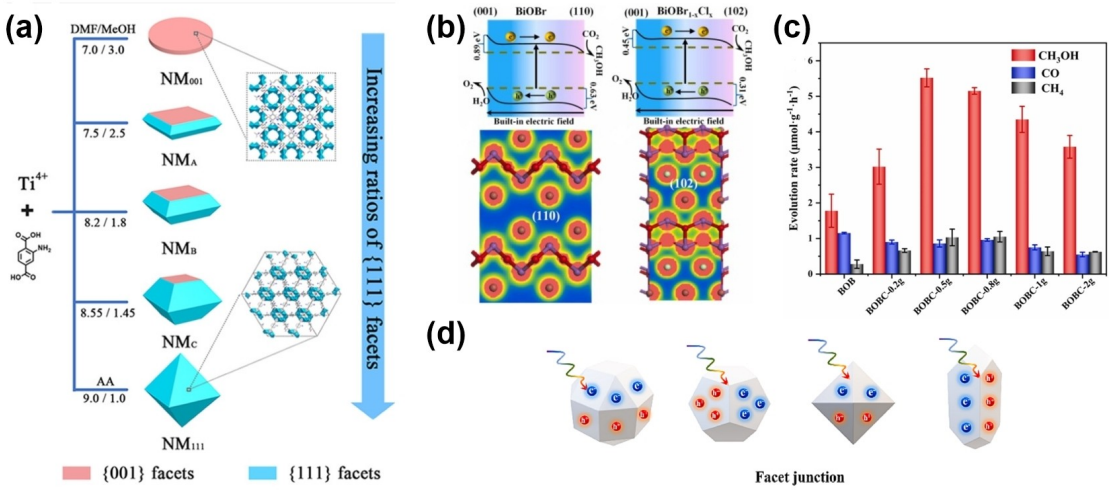

Figure 4. Effective photocatalyst design of facet engineering for simultaneous CO_2 reduction and H_2O oxidation. (a) Different facets of NH_2-MIL-125 (Ti) photocatalysts.[130] Copyright 2021, American chemical society. (b) Scheme of charge migration on BiOBr facet junction of (001)/(110) and (001)/(102) with their density of states and (c) the corresponding evolution rates.[105] Copyright 2024, Elsevier. (d) Facet junctions for the separation of photo-generated electrons and holes.[131] Copyright 2024, Elsevier.

Table 1. Summary of simultaneous photocatalytic CO_2 reduction and H_2O oxidation based on the strategies in the review.

Strategies	Photocatalysts	Reaction conditions	Product yields [$\mu mol\, g^{-1}\, h^{-1}$]		AQY [%]	Ref.
			CO_2 reduction	H_2O oxidation		
Vacancy design	V_s-SnS_2	5 mg catalyst 2 mL H_2O 300 W Xenon lamp	CO 25.71	O_2 9	–	[96]
	S-BiOCl	5 mg catalyst 1 mL H_2O UV-vis light	CO 49.76	–	–	[97]
	BNT-OVP	50 mg catalyst 5 mL H_2SO_4 1.3 g $NaHCO_3$ 300 W Xenon lamp	CO 20.9 CH_4 0.96	–	0.74 (365 nm)	[98]
	In/TiO_2-O_v	5 mg catalyst 1 mL H_2O 320–780 nm Xe lamp	CH_4 35.49	H_2O_2 20.1	–	[99]
	Sn/SnS_2	10 mg catalyst 10 mL H_2O 300 W Xe lamp (> 420 nm)	CO 295.06	–	–	[100]
	BOC-60	10 mg catalyst H_2O vapor 300 W Xe lamp 1 atm CO_2	CO 27.15	–	–	[101]
	V_{BiO}-BOB	30 mg catalyst 50 mL H_2O 300 W Xe lamp	CO 24.9	–	0.44 (380 nm)	[102]
	VBOC	20 mg catalyst 0.4 mL H_2O 300 W Xe lamp	CO 21.99	–	–	[103]
	BEG	40 mg catalyst 20 mL H_2O 300 W Xe lamp (> 420 nm)	CO 122.38	–	–	[104]
Facet design	BOBC-0.5	20 mg catalyst 20 mL H_2O 300 W Xe lamp (400–780 nm)	CH_3OH 5.52	–	-	[105]
	BiOBr-5	10 mg catalyst 0.2 mL H_2O 300 W Xe lamp	CO 6.5	-	1.10 (350 nm)	[106]
	$BiOIO_3$	50 mg catalyst 1.7 g $NaHCO_3$ 15 mL H_2SO_4 (4 M) 300 W Xe lamp	CO 5.42	–	–	[107]
	Ta_3N_5	100 mg catalyst 0.4 mL H_2O 300 W Xe lamp (> 420 nm)	CH_4 1.41	–	1.1 (500 nm)	[108]
	C_3N_4-PtCu	15 mg catalyst 1 mL H_2O 0.15 MPa CO_2 300 W Xe lamp (400–780 nm)	CH_4 7.33	–	–	[109]
Morphology design	BOC-VDWGs	50 mg catalyst 100 mL H_2O 300 W Xe lamp (> 400 nm)	CO 188.2	O_2 78.4	2.5 (400 nm)	[110]
	U-BOC	20 mg catalyst 50 mL H_2O 300 W Xe lamp	CO 21.4	–	–	[111]

Table 1. continued

Strategies	Photocatalysts	Reaction conditions	Product yields [μmol g^{-1} h^{-1}]		AQY [%]	Ref.
			CO_2 reduction	H_2O oxidation		
	2 Ag-BWO	20 mg catalyst 0.1 mL H_2O 300 W Xe lamp	CO 19.5	–	0.37 (350 nm)	[112]
	TBHO	20 mg catalyst 15 mL H_2O 25 W UV-LED	CO 29.1	–	–	[113]
	NST	10 mg catalyst 20 μL H_2O 1 atm CO_2 300 W Xe lamp	CH_4 147.2	–	–	[114]
Adjacent redox site construction	$Cu_{0.8}Au_{0.2}/TiO_2$	2 mg catalyst 0.2 mL H_2O 300 W Xe lamp	CH_4 3578.9	–	–	[115]
	$Cu_1/N_{2C}V$-CN-0.5	5 mg catalyst 0.2 mL H_2O 105 KPa	CO 11.12	–	–	[116]
	$AuCu/PbTiO_3/MnO_x$	20 mg catalyst 10 mL H_2O 320–780 nm (100 mW cm^{-2})	CO 23.9	–	–	[117]
	Ag_1/TiO_2	5 mg catalyst 0.2 mL H_2O 300 W Xe lamp	CH_4 46	–	–	[118]
	Rh–Ru/$NaTaO_3$:Sr	1.5 g catalyst 350 mL H_2O 400 W Hg lamp UV	CH_4 1.44	O_2 14	0.016 (270 nm)	[119]
	TPE-PT	20 mg catalyst 1 mL H_2O 300 W Xe lamp	CH_4 10.6	H_2O_2 350	0.8 (420 nm)	[34]
	Cu-SA/D-ZIS	10 mg catalyst 0.3 mL H_2O 300 W Xe lamp (> 420 nm)	CO 112.5	O_2 52.3	–	[92]
	Pd/CeO_2	5 mg catalyst 10 mL H_2O 300 W Xe lamp	CH_4 41.6	–	–	[120]
Z-scheme heterojunction development	$C_3N_4/Bi_4O_5I_2$	0.1 g catalyst 5 mL H_2SO_4 + $NaHCO_3$ 300 W Xe lamp (> 400 nm)	CO 45.6	–	–	[121]
	α-Fe_2O_3/Amine-RGO/$CsPbBr_3$	CO_2 + vapor H_2O 150 W Xe lamp (> 420 nm)	CO + CH_4 469.16	–	–	[122]
	Cu_2O–Pt/SiC/IrO_x	CO_2 + H_2O 150 mg catalyst 300 W Xe lamp (> 420 nm)	HCOOH 896.7	O_2	1.44	[123]
	WO_3/C_3N_4	0.27 MPa CO_2 0.5 mL H_2O 3 mg catalyst	CO + CH_4 12.0	–	–	[124]
	In_2O_3/Nb_2O_5	CO_2 0.3 mL H_2O 30 mL acetonitrile 10 mg catalyst	CO 109.6	–	–	[125]

In addition, different facets of the photocatalyst would affect the migration direction of photogenerated electrons and holes, leading to the spatial separation of oxidation and reduction reactions. For example, the junctions with different facets were fabricated, suggesting that the diverse exposed facets allowed the charges to migrate to the primary and

common facets, thereby exhibiting different reactivities, i.e., the performance of (001)/(102) junction was superior to that of (001)/(110) junction (Figure 4b and 4c).[105] Based on this advantage, it is possible to engineer facets on the photocatalysts, which regulates the migration of photogenerated electrons and holes to different crystal facets,[131] thereby simultaneously promoting the CO_2 reduction and H_2O oxidation on different facets, in order to improve the overall reaction efficiency, as illustrated in Figure 4d.

3.1.3. Morphology

Another method conducive to promoting photo-generated charge separation for efficient CO_2 reduction and H_2O oxidation is the construction of distinctive morphologies. It has been reported that the design layers for two-dimensional materials are beneficial for the promoting the photogenerated charge transfer.[110] As is shown in Figure 5a, the ultrathin BiOCl nanosheets composed of rich van der Waals gaps were developed, and exhibited 188.2 μmol g^{-1} h^{-1} CO production, superior to those of bulk crystals, which was resulted from the excellent performance of H_2O oxidation on the ultrathin BiOCl nanosheets (Figure 5b), furthermore, the transient photocurrent responses suggested that the enhanced charge-hole separation efficiency was beneficial for both CO_2 reduction and H_2O oxidation in this pure water system.

In addition, the photocatalyst with a core-shell structure is able to enhance the separation of photogenerated electrons and holes, and thus the overall photocatalytic reaction successfully achieves. For example, Yuan et al.[132] developed a core-shell nanotube and illustrated in Figure 5c, where the Co_3O_4 core acted as a site for the hole accumulation to the efficient H_2O oxidation, and the SiO_2 shell as a proton membrane separated protons from the oxidation sites to the reduction sites for CO_2 reduction (Figure 5d). Similarly, a mesoporous silica photocatalyst with Co-O–Zr species and IrO_x nanoclusters in its pores has a superior ability for simultaneous H_2O oxidation and CO_2 reduction,[133] in which a synergistic interaction for H_2O oxidation on IrO_x and a metal-to-metal charge transfer from Co-O–Zr to IrO_x for CO_2 reduction was achieved, as shown in Figure 5e and 5f. To date, the morphology construction is usually conducive to the enhanced photogenerated charge transfer or the effective separation of the holes and electrons, while the difficulty of molecular diffusion of CO_2 and H_2O is limited, especially in the porous materials. Based on the different dynamic molecular sizes of CO_2 and H_2O, the consideration of reactant molecule diffusion on the morphology design is necessary for the photocatalytic CO_2 reduction in pure H_2O.

3.2. Adjacent Redox Site Construction

For the photocatalytic CO_2 reduction in pure H_2O, the construction of redox sites, where the reduction site is designated for CO_2 adsorption and activation, and the oxidation site for H_2O, is an effective approach to improve the overall photocatalysis. Due to the distance limitation of proton transport after H_2O dissociation, it is necessary to design adjacent redox sites, similar to the challenges encountered in proton exchange membranes in electrolysis.[134] Therefore, various photocatalysts with adjacent redox sites are synthesized for simultaneous photocatalytic CO_2 reduction and H_2O oxidation.

Owing to the excellent properties of electron transfer and hydrogen-proton overflow, noble metals have been used as redox photocatalysts. For instance, Yu et al.[115] fabricated Cu single atoms (SAs) and Au–Cu alloy nanoparticles (NPs) on the TiO_2 support through a facile photodeposition method. In the reaction, the photoexcited electrons generated by TiO_2 were

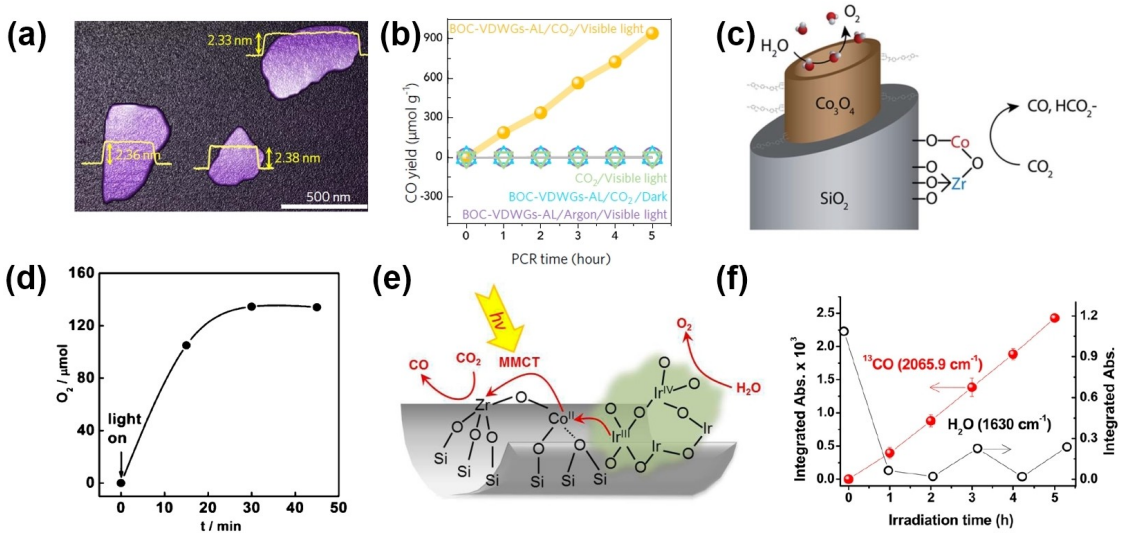

Figure 5. Effective photocatalyst design of morphology engineering for simultaneous CO_2 reduction and H_2O oxidation. (a) AFM image for BOC-VDWGs-AL, and (b) CO yields in the different reaction conditions.[110] Copyright 2021, Springer Nature. (c) Reaction sites of Co_3O_4-SiO_2 core-shell nanotube, and (d) the O_2 evolution determined by the mass spectroscopy.[132] Copyright 2024, The Royal Society of Chemistry. (e) A charge transfer from Co-O–Zr to IrOx in light and (f) kinetics of ^{13}CO formation and H_2O absorbed on ZrOCo-IrO_x.[133] Copyright 2014, American chemical society.

transferred to the Cu SA site to participate in CO_2 reduction, while the holes trapped by the AuCu alloy were used for the H_2O oxidation to produce O_2 (Figure 6a), and the in situ deposited materials exhibited outstanding synergistic catalytic performances and achieved high yields. Duan et al.[116] designed multiple active sites on $Cu_1/N_{2C}V$-CN, where the Cu single site promoted CO_2 conversion, while the two-coordinated N vacancies facilitated H_2O dissociation. Taking advantage of the dual-site effect, the performance was significantly improved with a yield rate of 11.12 $\mu mol\,g^{-1}\,h^{-1}$ and a CO selectivity of 98.5 %. In addition, a similar spatially separated redox photocatalyst is also achieved. The AuCu and MnO_x NPs were deposited on oppositely polarized facets of $PbTiO_3$, which were used for $CO_2 \rightarrow CO$ and $H_2O \rightarrow O_2$, respectively. The improved charge separation efficiency and lower rate-limiting-step energy barriers for CO_2 reduction and H_2O oxidation resulted in an excellent performance (Figure 6b).[117] The Ag_1/TiO_2 nanocrystal was also fabricated to realize the separated sites.[118] As shown in Figure 6c, the single Ag atom acted as a site for CO_2 adsorption and stabilized the *CO intermediate, while the adjacent Ti site contributed to the dissociation of H_2O and provision of active hydrogen, with the optimized adsorption energies of CO (−1.06 eV) and H_2O (−1.66 eV) in Figure 6d.

Among the energy-rich C1 products in the photocatalytic CO_2 reduction, CH_4 product has the highest heat of combustion at 890 $kJ\,mol^{-1}$, and attracts more attention. In general, the noble metal co-catalysts as active sites are required, and their highly selective CH_4 product is attributed to stronger coordination between *CO and metal sites to further reduction products. Soontornchaiyakul et al.[119] reported a Rh–Ru cocatalyst modified on Sr-$NaTaO_3$, which was able to convert CO_2 to CH_4 using H_2O as a proton donor (Figure 7a). For Sr-$NaTaO_3$, negligible CO or CH_4 products were detected, after Rh–Ru decoration, the appearance of CH_4 product indicated that the Rh–Ru cocatalyst served as an active site for CO_2 reduction. Moreover, the Pd-doped CeO_2 nanosheets were fabricated with the presence of $Pd^{\delta+}$ ($2 < \delta < 4$) and Ce^{3+}-O_v. In situ FI-TR showed that $Pd^{\delta+}$ sites could participate in H_2O oxidation and promote the formation of active hydrogen and subsequent hydrogenation steps of intermediates (Figure 7b).[120]

However, the noble metal-based photocatalytic active centers are often expensive, and their limited resources result in higher costs and hinder a wider application for CH_4 production. Therefore, the non-noble metals or free-metals consisting of renewable and cheap resources are used for the photocatalytic CO_2 reduction with H_2O. Li et al.[135] incorporated Mn into Co_3O_4 as a cocatalyst, where the Mn sites tended to accumulate vacancies for H_2O oxidation, and the adjacent Co sites participated in the activation and reduction of CO_2, as illustrated in Figure 7c. A heterometallic cluster catalyst of MCOF-Ti_6Cu_3 with spatially separated redox clusters was designed and synthesized, and Cu_3 clusters for CO_2 reduction and Ti_6 clusters for H_2O oxidation,[136] which exhibited an excellent HCOOH yield rate of 169.8 $\mu mol\,g^{-1}\,h^{-1}$, superior to most reported catalysts. In addition, single atom Cu on $ZnIn_2S_4$ nanosheets with rich Zn and S vacancies, which facilitated O–H cleavage in H_2O oxidation and further for O–H bonding in *COOH intermediate leading to about 6 times compared to pure $ZnIn_2S_4$ nanosheets in the photocatalytic CO_2 reduction.[92] Furthermore, our recent research has successfully synthesized a metal-free photocatalyst with a novel electron acceptor 4,5,9,10-pyrenetetrone (PT) and electron donor tetraphenyl ethylene (TPE) as the active sites for CO_2 and H_2O in the adjacent redox sites, respectively. This was the first time that CH_4 and H_2O_2 were simultaneously produced

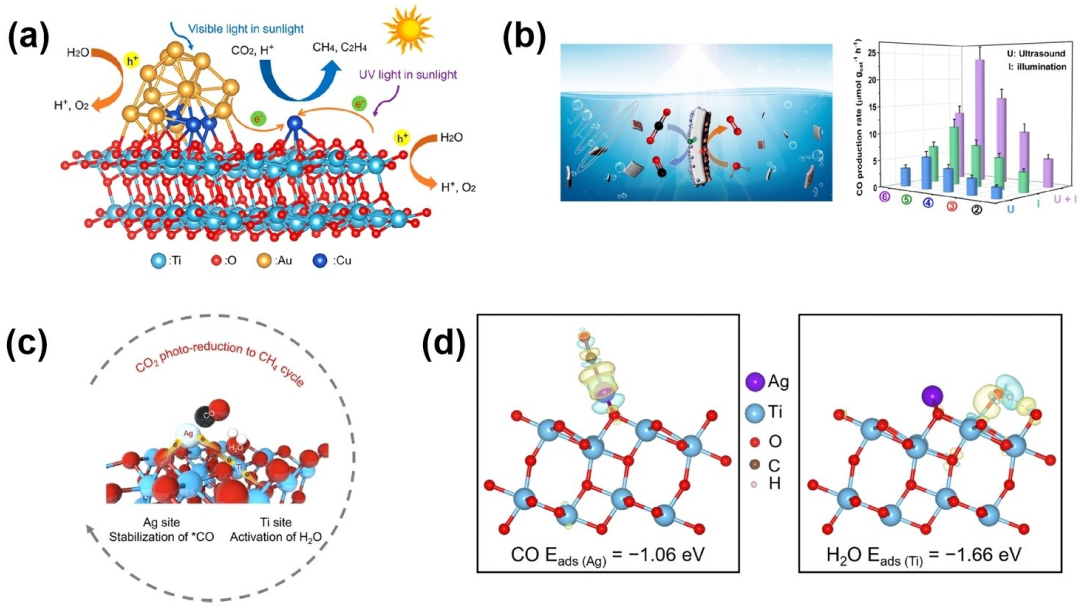

Figure 6. Constructions of adjacent redox sites for promoted photocatalytic CO_2 reduction and H_2O oxidation. (a) Cu single atom and Au–Cu alloy NPs/TiO_2.[115] Copyright 2021, American chemical society. (b) CO evolution rates on AuCu/$PbTiO_3$/MnO_x.[117] Copyright 2023, American chemical society. (c) Ag site for *CO stabilization and Ti site for H_2O activation, and (d) charge density difference of CO and H_2O adsorption on Ag/TiO_2, respectively.[118] Copyright 2024, The Royal Society of Chemistry.

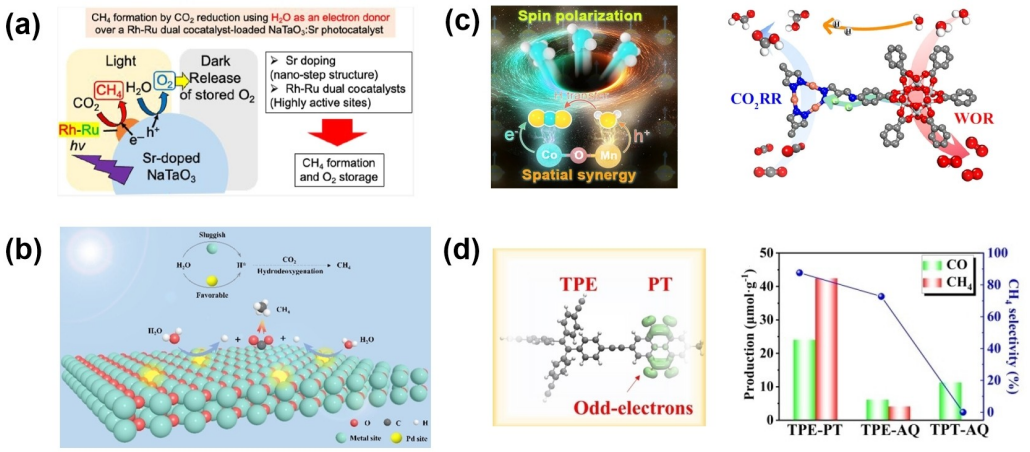

Figure 7. Adjacent redox site constructions. (a) Rh–Ru dual-site cocatalyst on Sr-$NaTaO_3$.[119] Copyright 2023, American chemical society. (b) H_2O activation on $Pd^{\delta+}$-CeO_2 to offer *H species.[120] Copyright 2022, Wiley-VCH. (c) Co-O–Mn structure with the spatial synergy for both CO_2 reduction and H_2O oxidation.[135] Copyright 2024, American chemical society. (d) A metal-free TPE-PT photocatalyst with the odd-electron density through TD-DFT, and the photocatalytic CO_2 reduction performances of TPE-PT, TPE-AQ, and TPT-AQ in pure water system.[34] Copyright 2023, Wiley-VCH.

using solar energy under non-sacrificial ambient conditions, where the excited odd electrons were located in PT moieties for CO_2 reduction, providing CH_4 production of 10.6 $\mu mol\,g^{-1}\,h^{-1}$ under the non-sacrificial condition (Figure 7d).[34]

3.3. Z-Scheme Heterojunction Development

The strategy of Z-scheme heterojunction development is one of the most effective means to improve photocatalytic CO_2 performance, because the greater the difference in the potentials between the band edges and the redox reactions, the stronger the driving force for CO_2 reduction (CO_2RR) and H_2O oxidation (WOR). For example, the Z-scheme g-C_3N_4/$Bi_4O_5I_2$ heterojunction showed that the electrons at the more negative CB edge of $Bi_4O_5I_2$ and holes at the more positive VB edge of g-C_3N_4 were beneficial for CO_2RR and WOR, respectively, compared to the Type II heterojunction (Figure 8a).[121]

In general, Z-scheme heterojunctions are divided into the direct and indirect Z-scheme. The indirect Z-scheme heterojunctions usually use ionic and solid-state electron mediators. A PVK-based Z-scheme heterojunction was reported,[122] where the electrons transferred from α-Fe_2O_3 to $CsPbBr_3$ were constructed to enhance charge separation and prolong carrier lifetime, with a stable product yield rate of 469 $\mu mol\,g^{-1}\,h^{-1}$. In addition, a Cu_2O–Pt/SiC/IrO_x composite was constructed to form the indirect Z-scheme system, spatially separating reduction and oxidation sites by a proton membrane (Figure 8b), and the yield rates of HCOOH and O_2 reached up to 896.7 $\mu mol\,g^{-1}\,h^{-1}$ and 440.7 $\mu mol\,g^{-1}\,h^{-1}$, respectively.[123]

Although many indirect Z-scheme heterojunctions have been constructed, which contribute to promote the overall

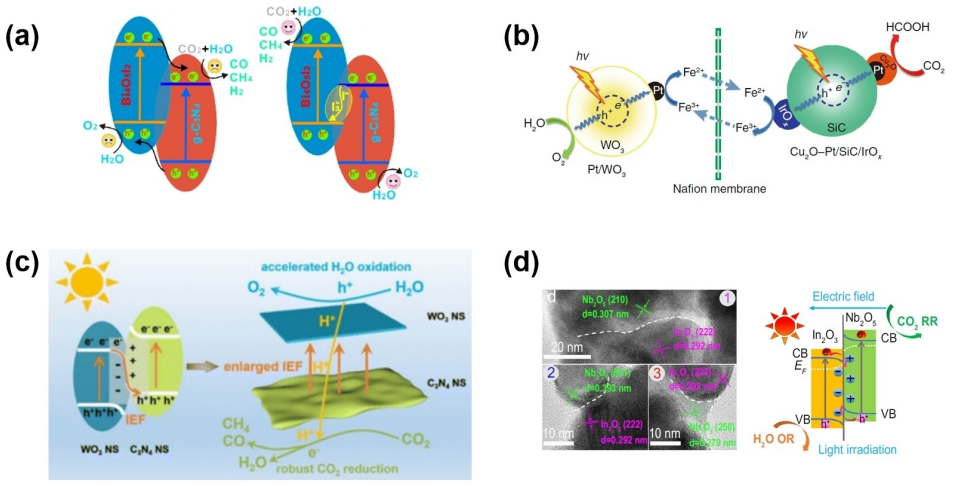

Figure 8. Z-scheme heterojunctions for promoted photocatalytic CO_2 reduction and H_2O oxidation. (a) g-C_3N_4/$Bi_4O_5I_2$.[121] Copyright 2016, Elsevier. (b) the separated redox system of Cu_2O–Pt/SiC/IrO_x.[123] Copyright 2020, Springer Nature. (c) WO_3/C_3N_4 nanosheets.[124] Copyright 2024, The Royal Society of Chemistry. (d) HRTEM image and the heterojunction formation of In_2O_3/Nb_2O_5.[125] Copyright 2024, Springer Nature.

photocatalytic efficiency of CO_2RR and WOR, the electron transfer on the mediator causes some problems, such as the complex preparation, slower transfer at the interface. Therefore, a direct Z-scheme heterojunction has been constructed. Song et al.[124] developed a WO_3/C_3N_4 Z-scheme heterojunction with C_3N_4 as CO_2RR active center and WO_3 as WOR site, which accelerated the sluggish kinetics (Figure 8c). Deng et al.[125] fabricated the In_2O_3/Nb_2O_3 heterojunction through a one-step electrospinning method to enable the intimate coupling of the two-phase interfaces, thereby forming well-defined heterojunctions, where different Fermi levels (E_F) of Nb_2O_5 and In_2O_3 promoted the formation of a direct Z-scheme heterojunction (Figure 8d). Furthermore, the $TiO_2/CsPbBr_3$ heterojunctions were synthesized by a facile electrostatic-driven self-assembly approach (Figure 9h), which effectively facilitated charge transfer, separated photogenerated electron-hole pairs, and maintained high redox potential for CO_2 reduction.[137]

Therefore, the development of Z-scheme heterojunction by coupling two suitable materials is an effective strategy for the efficient overall photocatalytic CO_2RR and WOR. However, the selection of suitable materials is still a challenging problem that requires a theoretical guidance.

4. Methods for Photocatalytic Mechanism Exploration

For the photocatalytic mechanism of the CO_2 reduction by H_2O oxidation, the determination of reaction intermediates to accurately evaluate the products and selectivity is of great importance. Generally, in situ electron paramagnetic resonance (EPR), in situ Raman, in situ diffuse reflectance infrared Fourier transform spectroscopy (DRIFTS), and density functional theory (DFT) calculations are used to explore the mechanism, in which the adsorption sites on the photocatalyst for CO_2 and H_2O, the generated intermediates, the corresponding formation energies, and the thermodynamical rate-determining step would be revealed. Furthermore, the reaction process of photocatalytic CO_2 reduction is related multi-electron transfer after excitonic dissociation, which is usually investigated by the Femtosecond-transient absorption (fs-TA) spectra. Therefore, the advanced characterization methods of the photocatalytic CO_2 reduction in the water system primarily include 1) in situ EPR, in situ Raman and DRIFTS, and DFT calculations for the reaction intermediates; 2) fs-TA spectra for the excited state dynamics of photocatalysts.

4.1. Reaction Intermediate Detection

4.1.1. In Situ EPR

In situ EPR is currently one of the most effective means of describing the photo-excited radicals to reveal the active sites and free radical intermediates in light. It allows the generation, accumulation, and consumption of active species under reaction conditions, or the structural evolution of catalysts to be observed. As shown in Figure 9a, in a metal-free photocatalyst of TPE-PT, after the photoexcitation, the EPR signal was observed at a certain g value (g = 2.0047), which was ascribed to the oxygen centered radical on the TPE-PT photocatalyst, with a long lifetime after extinction of light, typically considered as the active site for CO_2 activation.[34] In addition, in situ EPR was performed under different conditions to confirm the adsorption site. It was found that the signal of the oxygen-centered radical decreased when the condition was changed from He to CO_2 atmosphere, which served to trap and activate CO_2 (Figure 9b).[34] Moreover, other reaction free radical intermediates with unpaired electrons, such as $\cdot O_2^-$, $\cdot OH$, $\cdot CO_2^-$, etc.,

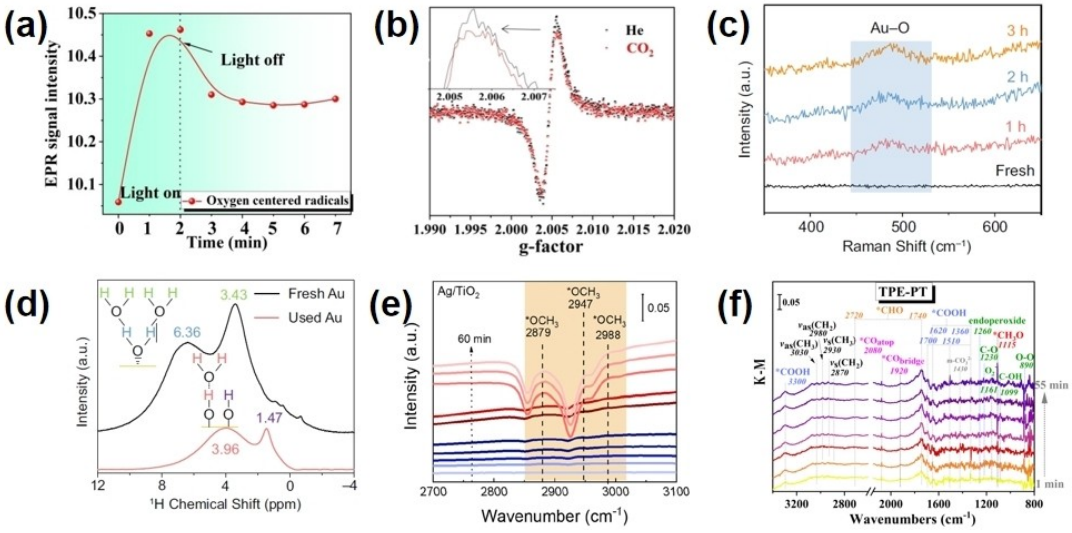

Figure 9. Advanced methods for mechanism exploration. (a) In situ EPR of TPE-PT under light irradiation and afterward turning off light and (b) in situ EPR spectra of TPE-PT under He or CO_2 conditions.[34] Copyright 2023, Wiley-VCH. (c) In situ Raman spectra of Au NPs with different photocatalytic reaction times, and (d) ^{1}H ssMAS-NMR spectra of Au samples before and after CO_2RR.[91] Copyright 2022, Springer Nature. (e) In situ DRIFTS of Ag_1/TiO_2.[118] Copyright 2024, The Royal Society of Chemistry. (f) In situ DRIFTS of CO_2 and H_2O adsorption under light irradiation of TPE-PT.[34] Copyright 2023, Wiley-VCH.

also could also be detected and analyzed qualitatively and quantitatively by the in situ EPR method, which is beneficial for understanding the reaction process.

4.1.2. In Situ Raman and DRIFTS

The photocatalytic CO_2 reduction by H_2O oxidation is a multi-step reaction, resulting in various intermediates after the electron activation and proton transfer. Detection of the reaction intermediates from the conversion of CO_2 and H_2O is facilitated to explore the mechanism of reaction activity and selectivity. In situ Raman and DRIFTS are useful methods, in which the changes in the dipole moment or polarization would be observed. For example, the activation sites for H_2O adsorption on the photocatalyst were found by the in situ Raman spectra and ^1H NMR, which showed that Au–O and AuOH-H_2O bond were formed during the reaction, providing evidence that Au served as H_2O activation sites (Figure 9c and 9d).[91]

Furthermore, in situ DRIFTS effectively describe the process of adsorption-activation-accumulation-consumption of the intermediates on the photocatalyst surface (Figure 9e),[118] providing compelling evidence for the investigation of the reaction mechanism, including of the selectivity of the products. For example, we recently has reported that there was a difference in CH_4 selectivity and activity between TPE-PT and TPT-AQ photocatalysts. In the in situ DRIFTS of CO_2 and H_2O adsorption under light irradiation (Figure 9f), it was observed that the peak (about 1850 cm^{-1}) assigned to C=O of cyclic ester was present only on TPE-PT, proving that the cyclic carbonate was a key intermediate for the highly-selective CH_4 production. In addition, on TPT-AQ, a stronger peak of $C{=}NH^+$ (1540 cm^{-1}) for H_2O adsorption was not conducive to subsequent oxidation, leading to poor activity of another half reaction of CO_2 reduction.[34]

4.1.3. DFT Calculations

In the investigation of photocatalytic reaction process, the DFT calculations can be used to determine the activation energies required for each of the hydrogenation elementary steps, providing a thermodynamic explanation for the improved performance.[120] In DFTcalculations, the primary focus is on the ground state properties of a system. However, the interactions between ground and excited states are often considered through methods like Time-Dependent DFT (TD-DFT), which extends the standard DFT framework to handle excited states. TD-DFT allows for the calculation of electronic excitations by incorporating time-dependent perturbations. This helps to understand how the system responds to external fields and provides insights into optical properties and excitation energies. In addition, the activation energy of the rate-determining step can also be calculated, and thus is related to the reaction performance. For instance, Gao et al.[138] calculated the formation energies of various transition states in the C–C coupling pathways, in order to elucidate the reaction steps and final products (Figure 10a). Furthermore, the formation energies of different intermediates on the photocatalyst surface would affect the reaction selectivity, such as *COOH intermediate for CH_4 produce, *OCHO intermediate for HCOOH product. Ren et al.[139] employed theoretical calculations to obtain the energies of different intermediates and thereby proposed the pathways for synthesis of multi-carbon products. That was, they identified the optimal materials for photocatalysis through the free energy, as shown in Figure 10b and c.

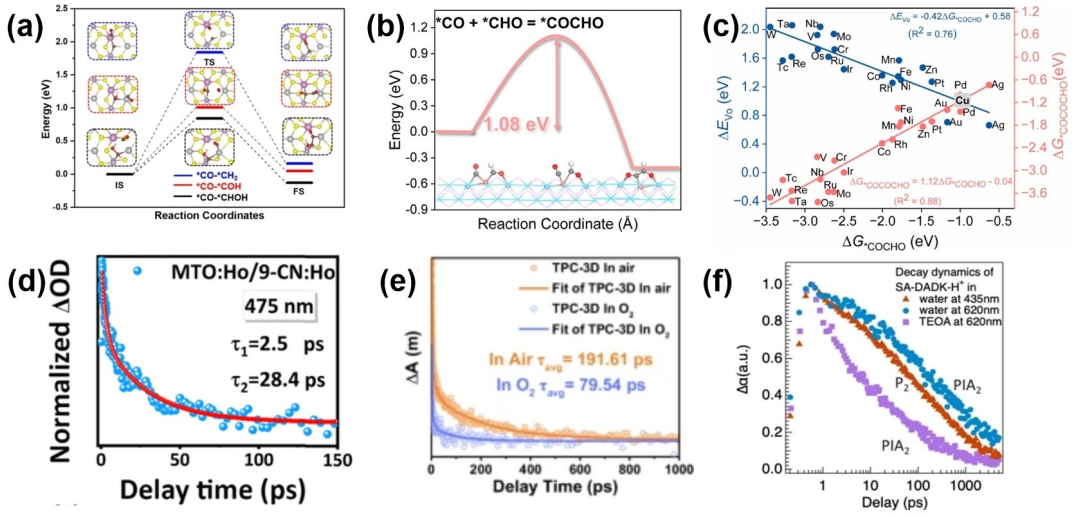

Figure 10. The application of DFT calculations and fs-TA spectra for mechanism exploration. (a) Three possible pathways of C–C coupling over $AgInP_2S_6$ containing V_s.[138] Copyright 2021, Springer Nature. (b) Minimum energy pathways of the C–C coupling through *CO and *CHO, and (c) the linear relation between ΔE_{Vo} and $\Delta G_{*COCOCHO}$ (adsorption free energy).[139] Copyright 2023, American chemical society. (d) The fs-TA spectra of MTO:Ho/CN:Ho using a 365 nm laser.[140] Copyright 2024, The Royal Society of Chemistry. (e) Comparison of TA kinetic profiles at 1000 nm under air and O_2 conditions, respectively.[142] Copyright 2024, Springer Nature. (f) TA decay dynamics of SA-DADK-H^+.[141] Copyright 2024, Wiley-VCH.

The DFT provides a good balance between accuracy and computational cost for ground state properties. It is widely applicable to various systems and provides a solid foundation for predicting material properties. However, it may struggle with strongly correlated electron systems and may not capture all types of electronic excitations accurately. Moreover, to date, most reports on the mechanism of photocatalytic CO_2 reduction have focused on the carbonate intermediates, while the reaction intermediates of H_2O oxidation are received less attention. Future advances in characterization techniques will provide insight into the role of H_2O activation in enhancing the overall reaction.

4.2. Excited-State Dynamics Determination (fs-TA Spectra)

In addition to studying the reaction intermediates, the investigation of the electron transfer mechanism and the electron withdrawal ability after excitonic dissociation are also important to the photocatalytic reduction of CO_2 by H_2O. Femtosecond transient absorption (fs-TA) spectroscopy is a critical tool for ultrafast dynamics studies, combining femtosecond time-resolved pump-probe techniques with absorption spectroscopy. This femtosecond time-resolved transient absorption spectroscopy provides information on the evolution of the absorption of the excited states. For example, An et al.[140] designed Ho single atom modified $Mg_{1.2}Ti_{1.8}O_5$/g-C_3N_4, which had a longer lifetime than that of CN:Ho (Figure 10d). Huang et al. proposed a strategy that the interlayer transfer of the photocatalysts was inhibited through the rapid dissociation of polarons into free charges, and the TA results showed that the O_2 atmosphere could not penetrate into the interior of the 2D photocatalyst to improve the carrier lifetime (Figure 10e). In addition, Zhu et al.[141] designed the protonation of N atoms on the pyridine rings of the photocatalysts, and the fs-TA spectra showed the effects on the exciton behavior, suggesting that the unsymmetric protonation decreased the exciton binding energy and increased charge carrier density, both of which were beneficial for the exciton separation and transport (Figure 10f). Therefore, the fs-TA spectroscopy is a key technique for investigating optical properties, such as excited state dynamics which play an important role in revealing the fundamental mechanisms of charge carrier migration in semiconductor materials.

5. Summary and Outlook

The field of simultaneous photocatalytic CO_2 reduction and H_2O oxidation under non-sacrificial ambient conditions is a highly effective and environmentally friendly approach to solving the global warming and fossil energy crisis. In this review, the recent advances and challenges of both half-reactions for CO_2 reduction and H_2O oxidation in photocatalysis are comprehensively reviewed. In addition, the strategies for photocatalyst design to improve the efficiency of both reduction and oxidation half-reactions are discussed in detail. Furthermore, the advanced characterization methods for exploring the reaction mechanisms including CO_2 and H_2O adsorption/activation, detection and construction of intermediates, and excited state dynamics, are summarized. However, despite significant study on photocatalytic reduction CO_2 by H_2O, some specific challenges and opportunities still exist in the theoretical investigation and practical application.

(i) Novel strategies to enhance H_2O oxidation to further promote a half-reaction of CO_2 reduction

The exploration of novel strategies to improve the kinetics and thermodynamics of the half-reaction of H_2O oxidation is imperative. Future investigations could focus on the synthesis of innovative bifunctional catalysts that can effectively realize the different requirements of both H_2O oxidation and CO_2 reduction. The design of photocatalysts would take advantage of advances in nanotechnology, surface chemistry and hybrid materials with optimal interfacial properties. In addition, the study of H_2O oxidation mechanisms in nature, such as those found in photosynthetic organisms, could provide biomimetic strategies to improve photocatalytic efficiency.

(ii) Accurate in situ characterization of active sites under the reaction conditions

Accurate in situ characterization of active sites under the reaction conditions remains a challenge, which is important for the photocatalyst optimization. The use of advanced spectroscopic techniques will be crucial in revealing the complex dynamics at these catalytic sites. Techniques such as in situ X-ray absorption spectroscopy (XAS) and EPR methods provide deep insights into the electronic structure and chemical environment of active sites during the photocatalytic process. Future advances may include the higher resolution and real-time detection which can provide accurate information on the catalytic processes under actual reaction conditions.

(iii) Integration of machine learning and neural networks for material prediction

The integration of machine learning (ML) and artificial neural networks (ANNs) is emerging as a potential approach to the prediction and design of photocatalytic materials. ML models can uncover the correlations that elude traditional analysis, potentially predicting novel materials with optimal properties for H_2O oxidation and CO_2 reduction. Future research should focus on expanding the datasets with high-quality experimental data and refining the algorithms, to improve accuracy in practical applications. The cooperation between computational scientists and experimentalists will be essential to apply these predictions into practical materials, which can be used in photocatalytic systems.

(iv) Effective separation and recycling of oxidation and reduction products

The effective separation and recycling of gaseous or liquid oxidation and reduction products from H_2O oxidation and CO_2 reduction in photocatalytic reactions is essential and remains a challenge. Generally, the products of H_2O oxidation are gaseous O_2 or liquid H_2O_2, and the products of CO_2 reduction are gaseous C1/C2 or liquid C2. Therefore, controlling the oxidation and reduction products with different states can reduce costs and aid application. In addition, there is still a formidable task to achieve cost-effective and efficient mass production. There-

fore, highly efficient catalysts, equipment, and practical technologies need to be developed in the future.

We believe that this review will guide future progress in photocatalytic CO_2 reduction by H_2O under non-sacrificial ambient conditions, with the aim of further development and practical applications in the field.

Acknowledgements

This work was supported by the National Natural Science Foundation of China (Grant 22336007, 22206209, 22106067, 62375120), the NSF of Guangdong Province (Grant 2022A1515011953), and Natural Science Foundation of Jiangsu Province (BK20240171).

Conflict of Interests

The authors declare no conflict of interest.

Data Availability Statement

Research data are not shared.

Keywords: Photocatalysis · Simultaneous half-reactions · CO_2 reduction · H_2O oxidation · Non-sacrificial ambient

[1] S. Solomon, G. K. Plattner, R. Knutti, P. Friedlingstein, *Proc. Natl. Acad. Sci. U. S.A* **2009**, *106*, 1704–1709.
[2] M. Vermeer, S. Rahmstorf, *Proc. Natl. Acad. Sci. U. S.A* **2009**, *106*, 21527–21532.
[3] M. C. Gao, J. X. Yang, T. Sun, Z. Z. Zhang, D. F. Zhang, H. J. Huang, H. X. Lin, Y. Fang, X. X. Wang, *Appl. Catal. B Environ. Energy* **2019**, *243*, 734–740.
[4] D. M. Etheridge, L. P. Steele, R. L. Langenfelds, R. J. Francey, J. M. Barnola, V. I. Morgan, *J Geophys Res-Atmos* **1996**, *101*, 4115–4128.
[5] Y. S. Yu, X. W. Zhang, J. W. Liu, Y. H. Lee, X. S. Li, *Energ Environ. Sci.* **2021**, *14*, 5611–5668.
[6] T. Inoue, A. Fujishima, S. Konishi, K. Honda, *Nature* **1979**, *277*, 637–638.
[7] Q. Wang, J. Warnan, S. Rodríguez-Jiménez, J. J. Leung, S. Kalathil, V. Andrei, K. Domen, E. Reisner, *Nat. Energy* **2020**, *5*, 703–710.
[8] D. Mateo, J. Albero, H. García, *Joule* **2019**, *3*, 1949–1962.
[9] Y. M. A. Wu, I. McNulty, C. Liu, K. C. Lau, Q. Liu, A. P. Paulikas, C. J. Sun, Z. H. Cai, J. R. Guest, Y. Ren, V. Stamenkovic, L. A. Curtiss, Y. Z. Liu, T. Rajh, *Nat. Energy* **2020**, *5*, 89–89.
[10] Y. O. Wang, E. Q. Chen, J. W. Tang, *ACS Catal.* **2022**, *12*, 7300–7316.
[11] X. Li, J. G. Yu, M. Jaroniec, X. B. Chen, *Chem. Rev.* **2019**, *119*, 3962–4179.
[12] D. D. Li, M. Kassymova, X. C. Cai, S. Q. Zang, H. L. Jiang, *Coord. Chem. Rev.* **2020**, *412*, 213262.
[13] E. Gong, S. Ali, C. B. Hiragond, H. S. Kim, N. S. Powar, D. Kim, H. Kim, S. I. In, *Energ Environ. Sci.* **2022**, *15*, 880–937.
[14] Y. J. Wang, T. He, *J. Mater. Chem. A* **2021**, *9*, 87–110.
[15] W. Zhu, X. Song, F. Liao, H. Huang, Q. Shao, K. Feng, Y. Zhou, M. Ma, J. Wu, H. Yang, H. Yang, M. Wang, J. Shi, J. Zhong, T. Cheng, M. Shao, Y. Liu, Z. Kang, *Nat. Commun.* **2023**, *14*, 5365.
[16] D. Li, C. J. Zhou, X. L. Shi, Q. Zhang, Q. Song, Y. M. Zhou, D. L. Jiang, *Mol. Catal.* **2022**, *526*, 112382.
[17] J. Y. Li, L. Yuan, S. H. Li, Z. R. Tang, Y. J. Xu, *J. Mater. Chem. A* **2019**, *7*, 8676–8689.
[18] S. J. Feng, J. Zhao, X. X. Liang, H. L. Li, C. Y. Wang, *Mol. Catal.* **2023**, *544*, 113205.
[19] J. Xiong, A. J. Yang, Q. Sun, H. X. Gao, H. Y. Zhang, Y. Mao, Z. W. Liang, *Mol. Catal.* **2023**, *547*, 113370.
[20] Z. W. Seh, J. Kibsgaard, C. F. Dickens, I. B. Chorkendorff, J. K. Norskov, T. F. Jaramillo, *Science* **2017**, *355*, eaad4998.
[21] R. Zhang, L. Pan, B. Guo, Z.-F. Huang, Z. Chen, L. Wang, X. Zhang, Z. Guo, W. Xu, K. P. Loh, J.-J. Zou, *J. Am. Chem. Soc.* **2023**, *145*, 2271–2281.
[22] P. F. Dong, X. Y. Xu, R. A. Luo, S. Yuan, J. Zhou, J. P. Lei, *J. Am. Chem. Soc.* **2023**, *145*, 15473–15481.
[23] Z. G. Liu, J. Y. Li, Z. Y. Chen, M. Y. Li, L. Z. Wang, S. Q. Wu, J. L. Zhang, *Appl. Catal. B Environ. Energy* **2023**, *326*, 122338.
[24] N. Y. Huang, H. He, S. J. Liu, H. L. Zhu, Y. J. Li, J. Xu, J. R. Huang, X. Wang, P. Q. Liao, X. M. Chen, *J. Am. Chem. Soc.* **2021**, *143*, 17424–17430.
[25] J. W. Tang, J. R. Durrant, D. R. Klug, *J. Am. Chem. Soc.* **2008**, *130*, 13885–13891.
[26] L. H. Gao, W. Y. Xiao, M. Y. Qi, J. Y. Li, C. L. Tan, Z. R. Tang, *Mol. Catal.* **2024**, *554*, 113858.
[27] L. Yuan, M. Y. Qi, Z. R. Tang, Y. J. Xu, *Angew. Chem. Int. Ed.* **2021**, *60*, 21150–21172.
[28] C. Han, Y. H. Li, J. Y. Li, M. Y. Qi, Z. R. Tang, Y. J. Xu, *Angew. Chem. Int. Ed.* **2021**, *60*, 7962–7970.
[29] Y. P. Liu, D. Y. Shen, Q. Zhang, Y. Lin, F. Peng, *Appl. Catal. B Environ. Energy* **2021**, *283*, 119630.
[30] W. J. Zhang, Y. Hu, L. B. Ma, G. Y. Zhu, Y. R. Wang, X. L. Xue, R. P. Chen, S. Y. Yang, Z. Jin, *Adv.Sci.* **2018**, *5*, 1700275.
[31] H. X. Mai, T. C. Le, D. H. Chen, D. A. Winkler, R. A. Caruso, *Chem.Rev.* **2022**, *122*, 13478–13515.
[32] S. Y. Fang, Y. H. Hu, *Chem. Soc. Rev.* **2022**, *51*, 3609–3647.
[33] S. Fang, M. Rahaman, J. Bharti, E. Reisner, M. Robert, G. A. Ozin, Y. H. Hu, *Nat. Rev. Methods Primers* **2023**, *3*, 61.
[34] W. X. Zou, Y. Y. Cheng, Y. X. Ye, X. Q. Wei, Q. Tong, L. Dong, G. F. Ouyang, *Angew. Chem. Int. Ed.* **2023**, *62*, e202313392.
[35] W. Q. Li, L. Jin, F. Gao, H. Q. Wan, Y. Pu, X. Q. Wei, C. Chen, W. X. Zou, C. Z. Zhu, L. Dong, *Appl. Catal. B Environ. Energy* **2021**, *294*, 120257.
[36] K. Li, B. S. Peng, T. Y. Peng, *ACS Catal.* **2016**, *6*, 7485–7527.
[37] S. L. Wang, M. Xu, T. Y. Peng, C. X. Zhang, T. Li, I. Hussain, J. Y. Wang, B. E. Tan, *Nat. Commun.* **2019**, *10*, 676.
[38] Y. Wang, X. T. Shang, J. N. Shen, Z. Z. Zhang, D. B. Wang, J. J. Lin, J. C. S. Wu, X. Z. Fu, X. X. Wang, C. Li, *Nat. Commun.* **2020**, *11*, 3043.
[39] Y. Pu, Y. D. Luo, X. Q. Wei, J. F. Sun, L. L. Li, W. X. Zou, L. Dong, *Appl. Catal. B Environ. Energy* **2019**, *254*, 580–586.
[40] X. Y. Meng, S. Y. Wang, C. C. Zhang, C. Z. Dong, R. Li, B. A. Li, Q. Wang, Y. Ding, *ACS Catal.* **2022**, *12*, 10115–10126.
[41] L. M. Sun, Y. Zhuang, Y. S. Yuan, W. W. Zhan, X. J. Wang, X. G. Han, Y. L. Zhao, *Adv. Energy Mater.* **2019**, *9*, 1902839.
[42] A. X. Deng, Y. Sun, Z. Q. Gao, S. G. Yang, Y. Z. Liu, H. He, J. Q. Zhang, S. M. Liu, H. Q. Sun, S. B. Wang, *Nano Energy* **2023**, *108*, 108228.
[43] P. P. Yu, N. Li, W. X. Zou, X. Q. Wei, J. W. Ji, L. Han, Y. D. Cai, W. Tan, B. Gao, L. Dong, *Chem. Eng. J.* **2023**, *451*, 138943.
[44] L. L. Zhang, W. H. Feng, B. Wang, K. Q. Wang, F. Gao, Y. Zhao, P. Liu, *Appl. Catal. B Environ. Energy* **2017**, *212*, 80–88.
[45] W. Zhao, Y. Feng, H. B. Huang, P. C. Zhou, J. Li, L. L. Zhang, B. L. Dai, J. M. Xu, F. X. Zhu, N. Sheng, D. Y. C. Leung, *Appl. Catal. B Environ. Energy* **2019**, *245*, 448–458.
[46] C. X. Zhang, C. F. Xie, Y. Y. Gao, X. P. Tao, C. M. Ding, F. T. Fan, H. L. Jiang, *Angew. Chem. Int. Ed.* **2022**, *61*, e202204108.
[47] R. Verma, R. Belgamwar, V. Polshettiwar, *ACS Materials Lett.* **2021**, *3*, 574–598.
[48] Y. Xin, K. F. Yu, L. T. Zhang, Y. R. Yang, H. B. Yuan, H. L. Li, L. B. Wang, J. Zeng, *Adv. Mater.* **2021**, *33*, 2008145.
[49] M. T. Pham, A. Hussain, D. P. Bui, T. M. T. Nguyen, S. J. You, Y. F. Wang, *Environ. Technol. Innov.* **2021**, *23*, 101755.
[50] Y. Kuramochi, O. Ishitani, H. Ishida, *Coord. Chem. Rev.* **2018**, *373*, 333–356.
[51] A. Perazio, G. Lowe, R. Gobetto, J. Bonin, M. Robert, *Coord. Chem. Rev.* **2021**, *443*, 214018.
[52] H. L. Li, J. K. Zhao, L. H. Luo, J. J. Du, J. Zeng, *Acc. Chem. Res.* **2021**, *54*, 1454–1464.
[53] J. Gu, F. Héroguel, J. Luterbacher, X. L. Hu, *Angew. Chem. Int. Ed.* **2018**, *57*, 2943–2947.
[54] W. Zhang, Y. Hu, L. Ma, G. Zhu, Y. Wang, X. Xue, R. Chen, S. Yang, Z. Jin, *Adv. Sci.* **2018**, *5*, 1700275.
[55] S. Nitopi, E. Bertheussen, S. B. Scott, X. Y. Liu, A. K. Engstfeld, S. Horch, B. Seger, I. E. L. Stephens, K. Chan, C. Hahn, J. K. Norskov, T. F. Jaramillo, I. Chorkendorff, *Chem.Rev.* **2019**, *119*, 7610–7672.
[56] Y. X. Pan, Y. You, S. Xin, Y. T. Li, G. T. Fu, Z. M. Cui, Y. L. Men, F. F. Cao, S. H. Yu, J. B. Goodenough, *J. Am. Chem. Soc.* **2017**, *139*, 4123–4129.

[57] X. Wei, X. Zhang, L. Jin, X. Yang, W. Zou, B. Gao, L. Dong, *Appl. Catal. B Environ. Energy* **2024**, *351*, 123957.
[58] S. F. Ji, Y. Qu, T. Wang, Y. J. Chen, G. F. Wang, X. Li, J. C. Dong, Q. Y. Chen, W. Y. Zhang, Z. D. Zhang, S. Y. Liang, R. Yu, Y. Wang, D. S. Wang, Y. D. Li, *Angew. Chem. Int. Ed.* **2020**, *59*, 10651–10657.
[59] R. A. Wang, M. J. Zhang, S. L. Zhang, J. Z. Zheng, Y. Q. Zeng, Y. Yang, J. Ding, X. Wu, Q. Zhong, *ACS Nano* **2023**, *17*, 24363–24373.
[60] C. X. Yin, X. Li, S. C. Sun, X. Q. Wei, Q. Tong, W. Tan, X. Wang, B. Peng, H. Q. Wan, L. Dong, *Chem. Commun.* **2024**, *60*, 3531–3534.
[61] X. Wang, H. Liao, W. Tan, W. Song, X. Li, J. Ji, X. Wei, C. Wu, C. Yin, Q. Tong, B. Peng, S. Sun, H. Wan, L. Dong, *ACS Appl. Mater. Interfaces* **2024**, *16*, 22089–22101.
[62] R. Long, Y. Li, Y. Liu, S. M. Chen, X. S. Zheng, C. Gao, C. H. He, N. S. Chen, Z. M. Qi, L. Song, J. Jiang, J. F. Zhu, Y. J. Xiong, *J. Am. Chem. Soc.* **2017**, *139*, 4486–4492.
[63] K. Kamada, J. Jung, T. Wakabayashi, K. Sekizawa, S. Sato, T. Morikawa, S. Fukuzumi, S. Saito, *J. Am. Chem. Soc.* **2020**, *142*, 10261–10266.
[64] H. Yu, C. Sun, Y. Xuan, K. Zhang, K. Chang, *Chem. Eng. J.* **2022**, *430*, 132940.
[65] F. Zhang, Y. H. Li, M. Y. Qi, Y. M. A. Yamada, M. Anpo, Z. R. Tang, Y. J. Xu, *Chem Catal.* **2021**, *1*, 272–297.
[66] F. K. Shang, Y. H. Li, M. Y. Qi, Z. R. Tang, Y. J. Xu, *Catal. Today* **2023**, *410*, 85–101.
[67] M. Y. Qi, Y. J. Xu, *Angew. Chem. Int. Ed.* **2023**, *62*, e202311731.
[68] S. T. Liu, B. L. Tian, X. Z. Wang, Y. M. Sun, Y. Q. Wang, J. Ma, M. N. Ding, *J. Phys. Chem. Lett.* **2022**, *13*, 9607–9617.
[69] S. Liu, B. Tian, X. Xu, X. Wang, P. Ran, Y. Sun, J. Wu, A. Qiu, F. Wang, L. Tang, J. Ma, M. Ding, *ACS Catal.* **2024**, 9476–9486.■■Kindly provide volume number.■■
[70] B. Sun, Z. Q. Li, D. F. Xiao, H. L. Liu, K. P. Song, Z. Y. Wang, Y. Y. Liu, Z. K. Zheng, P. Wang, Y. Dai, B. B. Huang, A. Thomas, H. F. Cheng, *Angew. Chem. Int. Ed.* **2024**, *63*, e202318874.
[71] W. H. Wang, X. S. Wang, Z. G. Ma, Y. Wang, Z. X. Yang, J. X. Zhu, L. Lv, H. Ning, N. Tsubaki, M. B. Wu, *ACS Catal.* **2023**, *13*, 796–802.
[72] W. S. Fang, W. Guo, R. H. Lu, Y. Yan, X. K. Liu, D. Wu, F. M. Li, Y. S. Zhou, C. H. He, C. F. Xia, H. T. Niu, S. C. Wang, Y. W. Liu, Y. Mao, C. Y. Zhang, B. You, Y. J. Pang, L. L. Duan, X. Yang, F. Song, T. Y. Zhai, G. X. Wang, X. P. Guo, B. Tan, T. Yao, Z. Y. Wang, B. Y. Xia, *Nature* **2024**, *626*, 86–91.
[73] Z. X. Tao, A. J. Pearce, J. M. Mayer, H. L. Wang, *J. Am. Chem. Soc.* **2022**, *144*, 8641–8648.
[74] M. Ma, K. Liu, J. Shen, R. Kas, W. A. Smith, *ACS Energy Lett.* **2018**, *3*, 1301–1306.
[75] W. J. Guo, G. F. Li, C. B. Bai, Q. Liu, F. X. Chen, R. Chen, *Nat. Commun.* **2024**, *15*, 1573.
[76] J. Feng, L. Wu, X. Song, L. Zhang, S. Jia, X. Ma, X. Tan, X. Kang, Q. Zhu, X. Sun, B. Han, *Nat. Commun.* **2024**, *15*, 4821.
[77] J. Bi, P. Li, J. Liu, S. Jia, Y. Wang, Q. Zhu, Z. Liu, B. Han, *Nat. Commun.* **2023**, *14*, 2823.
[78] J. W. Li, T. C. Xiang, X. Liu, M. N. Ghazzal, Z. Q. Liu, *Angew. Chem. Int. Ed.* **2024**, *63*, e202407287.
[79] S. T. Guo, Y. W. Du, H. H. Luo, Z. Y. Zhu, T. Ouyang, Z. Q. Liu, *Angew. Chem. Int. Ed.* **2024**, *63*, e202314099.
[80] Y. Yu, X. A. Dong, P. Chen, Q. Geng, H. Wang, J. Li, Y. Zhou, F. Dong, *ACS Nano* **2021**, *15*, 14453–14464.
[81] L. Liang, F. C. Lei, S. Gao, Y. F. Sun, X. C. Jiao, J. Wu, S. Qamar, Y. Xie, *Angew. Chem. Int. Ed.* **2015**, *54*, 13971–13974.
[82] Y. Zheng, A. Vasileff, X. L. Zhou, Y. Jiao, M. Jaroniec, S. Z. Qiao, *J. Am. Chem. Soc.* **2019**, *141*, 7646–7659.
[83] S. T. Guo, Z. Y. Tang, Y. W. Du, T. Liu, T. Ouyang, Z. Q. Liu, *Appl. Catal. B Environ. Energy* **2023**, *321*, 122035.
[84] R. Zhao, Z. Y. Zhu, T. Ouyang, Z. Q. Liu, *Angew. Chem. Int. Ed.* **2024**, *63*, e202313597.
[85] J. J. Walsh, C. R. Jiang, J. W. Tang, A. J. Cowan, *Phys. Chem.Chem. Phys.* **2016**, *18*, 24825–24829.
[86] H. N. Che, X. Gao, J. Chen, J. Hou, Y. H. Ao, P. F. Wang, *Angew. Chem. Int. Ed.* **2021**, *60*, 25546–25550.
[87] W. Liu, P. F. Wang, Y. H. Ao, J. Chen, X. Gao, B. H. Jia, T. Y. Ma, *Adv. Mater.* **2022**, *34*, e202313597.
[88] Q. Zhang, T. Wu, H. Che, C. Tang, B. Liu, Y. Ao, *Surf. Interfaces* **2024**, *47*, 104205.
[89] S. K. Yin, X. X. Zhao, E. H. Jiang, Y. Yan, P. Zhou, P. W. Huo, *Energy Environ. Sci.* **2022**, *15*, 1556–1562.
[90] Z.-F. Huang, J. Song, Y. Du, S. Xi, S. Dou, J. M. V. Nsanzimana, C. Wang, Z. J. Xu, X. Wang, *Nat. Energy* **2019**, *4*, 329–338.
[91] W. C. Shangguan, Q. Liu, Y. Wang, N. Sun, Y. Liu, R. Zhao, Y. X. Li, C. Y. Wang, J. C. Zhao, *Nat. Commun.* **2022**, *13*, 3894.
[92] W. Wang, W. Y. Zhang, C. Y. Deng, H. Sheng, J. C. Zhao, *Angew. Chem. Int. Ed.* **2024**, e202317969.■■Kindly provide volume number.■■
[93] A. Zagalskaya, V. Alexandrov, *ACS Catal.* **2020**, *10*, 3650–3657.
[94] H. Li, J. Shang, H. Zhu, Z. Yang, Z. Ai, L. Zhang, *ACS Catal.* **2016**, *6*, 8276–8285.
[95] B. Su, Y. Kong, S. Wang, S. Zuo, W. Lin, Y. Fang, Y. Hou, G. Zhang, H. Zhang, X. Wang, *J. Am. Chem. Soc.* **2023**, *145*, 27415–27423.
[96] S. Yin, X. Zhao, E. Jiang, Y. Yan, P. Zhou, P. Huo, *Energy Environ. Sci.* **2022**, *15*, 1556–1562.
[97] K. Yan, L. Chen, Y. Hu, T. Wang, C. Chen, C. Gao, Y. Huang, B. Li, *Nano Res.* **2024**, *17*, 1056–1065.
[98] H. J. Yu, F. Chen, X. W. Li, H. W. Huang, Q. Y. Zhang, S. Q. Su, K. Y. Wang, E. Y. Mao, B. T. Mei, G. D. Mul, T. Y. Ma, Y. H. Zhang, *Nat. Commun.* **2021**, *12*, 4594.
[99] C. Chen, L. Chen, Y. Hu, K. Yan, T. Wang, Y. Huang, C. Gao, J. Mao, S. Liu, B. Li, *J. Energy Chem.* **2023**, *86*, 599–608.
[100] H. Y. Zhang, L. Mao, J. Y. Wang, Y. Nie, Z. K. Geng, D. C. Zhong, X. Tan, J. H. Ye, T. Yu, *Small* **2024**, *20*, 2305727.
[101] X. Shi, X. A. Dong, Y. He, P. Yan, F. Dong, *Sci.Bull.* **2022**, *67*, 1137–1144-
[102] J. Di, C. Chen, C. Zhu, R. Long, H. L. Chen, X. Z. Cao, J. Xiong, Y. X. Weng, L. Song, S. Z. Li, H. M. Li, Y. J. Xiong, Z. Liu, *Adv. Energy Mater.* **2021**, *11*, 2102389.
[103] L. Wang, R. Wang, T. Qiu, L. Yang, Q. Han, Q. Shen, X. Zhou, Y. Zhou, Z. Zou, *Nano Lett.* **2021**, *21*, 10260–10266.
[104] Q. Yang, Y. Wang, Q. Tian, X. Li, A. Pan, M. Zhao, Y. Zhu, T. Wu, G. Fang, *J. Mater. Chem. A* **2024**, *12*, 7207–7214.
[105] L. Wang, C. H. Qiu, R. J. Chen, X. R. Chen, J. Ding, J. F. Zhang, H. Wan, G. F. Guan, *J. Alloys Compd.* **2024**, *985*, 174022.
[106] J. Meng, Y. Duan, S. Jing, J. Ma, K. Wang, K. Zhou, C. Ban, Y. Wang, B. Hu, D. Yu, L. Gan, X. Zhou, *Nano Energy* **2022**, *92*, 106671.
[107] F. Chen, H. Huang, L. Ye, T. Zhang, Y. Zhang, X. Han, T. Ma, *Adv. Funct. Mater.* **2018**, *28*, 1804284.
[108] C. Zhou, J. Zhou, L. Lu, J. Wang, Z. Shi, B. Wang, L. Pei, S. Yan, Y. Zhentao, Z. Zou, *Appl. Catal. B Environ. Energy* **2018**, *237*, 742–752.
[109] Q. Lang, Y. Yang, Y. Zhu, W. Hu, W. Jiang, S. Zhong, P. Gong, B. Teng, L. Zhao, S. Bai, *J. Mater. Chem. A* **2017**, *5*, 6686–6694.
[110] Y. B. Shi, J. Li, C. L. Mao, S. Liu, X. B. Wang, X. F. Liu, S. X. Zhao, X. Liu, Y. Q. Huang, L. Z. Zhang, *Nat. Commun.* **2021**, *12*, 5923.
[111] Y. Zhang, Z. Xu, Q. Wang, W. Hao, X. Zhai, X. Fei, X. Huang, Y. Bi, *Appl. Catal. B Environ. Energy* **2021**, *299*, 120679.
[112] L. Zhao, H. Hou, L. Wang, C. R. Bowen, J. Wang, R. Yan, X. Zhan, H. Yang, M. Yang, W. Yang, *Chem. Eng. J.* **2024**, *480*, 148033.
[113] C. Jia, B. Wan, W. Liu, L. Qi, X. Liu, X. Han, A. Gao, J. Liu, *Adv. Funct. Mater.* **2024**, *34*, 2311663.
[114] Z.-W. Wang, Q. Wan, Y.-Z. Shi, H. Wang, Y.-Y. Kang, S.-Y. Zhu, S. Lin, L. Wu, *Appl. Catal. B Environ. Energy* **2021**, *288*, 120000.
[115] Y. Y. Yu, X. A. Dong, P. Chen, Q. Geng, H. Wang, J. Y. Li, Y. Zhou, F. Dong, *ACS Nano* **2021**, *15*, 14453–14464.
[116] Y. Y. Duan, Y. Wang, W. X. Zhang, J. W. Zhang, C. G. Ban, D. M. Yu, K. Zhou, J. J. Tang, X. Zhang, X. D. Han, L. Y. Gan, X. P. Tao, X. Y. Zhou, *Adv. Funct. Mater.* **2023**, *33*, 2301729.
[117] G. D. Yang, S. H. Wang, Y. J. Wu, H. Zhou, W. Zhao, S. X. Zhong, L. C. Liu, S. Bai, *ACS Appl. Mater. Interfaces* **2023**, *15*, 14228–14239.
[118] C. Ban, Y. Wang, Y. Feng, Z. Zhu, Y. Duan, J. Ma, X. Zhang, X. Liu, K. Zhou, H. Zou, D. Yu, X. Tao, L. Gan, G. Han, X. Zhou, *Energy Environ. Sci.* **2024**, *17*, 518–530.
[119] W. Soontornchaiyakul, S. Yoshino, T. Kanazawa, R. Haruki, D. X. Fan, S. Nozawa, Y. Yamaguchi, A. Kudo, *J. Am. Chem. Soc.* **2023**, *145*, 20485–20491.
[120] Z. Q. Wang, J. C. Zhu, X. L. Zu, Y. Wu, S. Shang, P. Q. Ling, P. Z. Qiao, C. Y. Liu, J. Hu, Y. Pan, J. F. Zhu, Y. F. Sun, Y. Xie, *Angew. Chem. Int. Ed.* **2022**, *61*, e202203249.
[121] Y. Bai, L. Ye, L. Wang, X. Shi, P. Wang, W. Bai, P. K. Wong, *Appl. Catal. B Environ. Energy* **2016**, *194*, 98–104.
[122] Y. Jiang, J.-F. Liao, H.-Y. Chen, H.-H. Zhang, J.-Y. Li, X.-D. Wang, D.-B. Kuang, *Chem* **2020**, *6*, 766–780.
[123] Y. Wang, X. Shang, J. Shen, Z. Zhang, D. Wang, J. Lin, J. C. S. Wu, X. Fu, X. Wang, C. Li, *Nat. Commun.* **2020**, *11*, 3043.
[124] Z. Song, Q. Chen, Z. Sun, K. Chang, Z. Xie, Q. Kuang, *J. Mater. Chem. A* **2024** *12*, 14426–14436.
[125] X. Deng, J. Zhang, K. Qi, G. Liang, F. Xu, J. Yu, *Nat. Commun.* **2024**, *15*, 4807.

[126] M. Shi, G. N. Li, J. M. Li, X. Jin, X. P. Tao, B. Zeng, E. A. Pidko, R. G. Li, C. Li, *Angew. Chem. Int. Ed.* **2020**, *59*, 6590–6595.
[127] M. Li, S. X. Yu, H. W. Huang, X. W. Li, Y. B. Feng, C. Wang, Y. G. Wang, T. Y. Ma, L. Guo, Y. H. Zhang, *Angew. Chem. Int. Ed.* **2019**, *58*, 9517–9521.
[128] J. Z. Meng, Y. Y. Duan, S. J. Jing, J. P. Ma, K. W. Wang, K. Zhou, C. G. Ban, Y. Wang, B. H. Hu, D. M. Yu, L. Y. Gan, X. Y. Zhou, *Nano Energy* **2022**, *92*, 106671.
[129] L. W. Shan, J. C. Li, Z. Wu, L. M. Dong, H. T. Chen, D. Li, J. Suriyaprakash, X. L. Zhang, *Chem. Eng. J.* **2022**, *436*, 131516.
[130] X.-M. Cheng, X.-Y. Dao, S.-Q. Wang, J. Zhao, W.-Y. Sun, *ACS Catal.* **2021**, *11*, 650–658.
[131] Z. D. Wei, J. W. Yan, Y. C. Zhang, W. J. Fang, S. Wenfeng, *Chem. Eng. J.* **2024**, *483*, 149267.
[132] G. B. Yuan, A. Agiral, N. Pellet, W. Kim, H. Frei, *Faraday Discuss.* **2014**, *176*, 233–249.
[133] W. Kim, G. Yuan, B. A. McClure, H. Frei, *J. Am. Chem. Soc.* **2014**, *136*, 11034–11042.
[134] H. Lv, J. Chen, W. Zhou, X. Shen, C. Zhang, *Renew. Sust. Energ. Rev.* **2023**, *183*, 113394.
[135] M. Y. Li, S. Q. Wu, D. N. Liu, Z. C. Ye, L. J. Wang, M. Kan, Z. W. Ye, M. Khan, J. L. Zhang, *J. Am. Chem. Soc.* **2024**, *146*, 15538–15548.
[136] J. Zhou, J. Li, L. Kan, L. Zhang, Q. Huang, Y. Yan, Y. Chen, J. Liu, S.-L. Li, Y.-Q. Lan, *Nat. Commun.* **2022**, *13*, 4681.
[137] F. Xu, K. Meng, B. Cheng, S. Wang, J. Xu, J. Yu, *Nat. Commun.* **2020**, *11*, 4613.
[138] W. Gao, S. Li, H. He, X. Li, Z. Cheng, Y. Yang, J. Wang, Q. Shen, X. Wang, Y. Xiong, Y. Zhou, Z. Zou, *Nat. Commun.* **2021**, *12*, 4747.
[139] C. Ren, Q. Li, C. Ling, J. Wang, *J. Am. Chem. Soc.* **2023**, *145*, 28276–28283.
[140] J. An, S. Ge, G. Wang, H. Fu, *Energy Environ. Sci.* **2024**, *17*, 5039–5047.
[141] X. Zhu, Y. Jia, Y. Liu, J. Xu, H. He, S. Wang, Y. Shao, Y. Zhai, Y. Zhu, *Angew. Chem. Int. Ed.* **2024**, *63*, e202405962.
[142] Y. Huang, M. Shen, H. Yan, Y. He, J. Xu, F. Zhu, X. Yang, Y.-X. Ye, G. Ouyang, *Nat. Commun.* **2024**, *15*, 5406.

Manuscript received: July 11, 2024
Accepted manuscript online: October 1, 2024
Version of record online: ■■, ■■

REVIEW

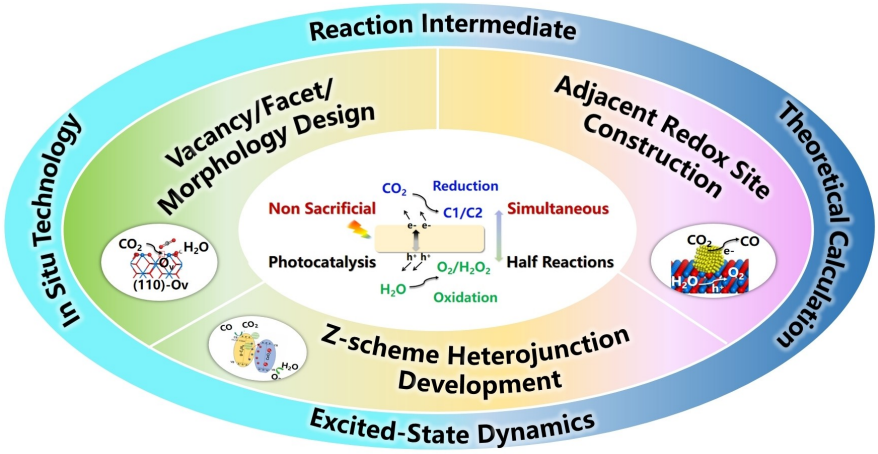

Q. Tong, Y. Tang, W. Zou, Y.-X. Ye, L. Dong, G. Ouyang**

1 – 18

Simultaneous Photocatalytic CO_2 Reduction and H_2O Oxidation Under Non-Sacrificial Ambient Conditions

83%

Dear Author, please provide a TOC text (about three short sentences, which summarize the content of your article). This text will appear together with the TOC figure on the first pages of the online issue, if your article will become part of this issue.

SPACE RESERVED FOR IMAGE AND LINK

Share your work on X! Chemistry – A European Journal promotes selected articles on X (formerly known as Twitter). Each article post contains the title, name of the corresponding author, a link to the article, selected handles and hashtags, and the ToC picture. If you, your team, or your institution have an X account, please include its handle @username below. We recommend sharing and interacting with these posts through your personal and/or institutional accounts to help increase awareness of your work! Please follow us @ChemEurJ.

ORCID (Open Researcher and Contributor ID)

Please check that the ORCID identifiers listed below are correct. We encourage all authors to provide an ORCID identifier for each coauthor. ORCID is a registry that provides researchers with a unique digital identifier. Some funding agencies recommend or even require the inclusion of ORCID IDs in all published articles, and authors should consult their funding agency guidelines for details. Registration is easy and free; for further information, see http://orcid.org/.

Qing Tong
Yu Tang
Weixin Zou
Yu-Xin Ye
Lin Dong
Gangfeng Ouyang http://orcid.org/0000-0002-0797-6036